DEPARTMENT OF PHYSICS, UNIVERSITY OF JYVÄSKYLÄ
RESEARCH REPORT No. 4/1980

HIGH-RESOLUTION STUDY OF E0 INTERNAL-PAIR TRANSITIONS FROM EXCITED 0^+ STATES IN $^{58, 60, 62}$Ni

BY
ARTO PASSOJA

Academic dissertation
for the Degree of
Doctor of Philosophy

Jyväskylä, Finland
April 1980

URN:ISBN:978-951-39-9912-4
ISBN 978-951-39-9912-4 (PDF)
ISSN 0075-465X

University of Jyväskylä, 2024

ISBN 951-678-335-X
ISSN 0075-465-X

DEPARTMENT OF PHYSICS, UNIVERSITY OF JYVÄSKYLÄ
RESEARCH REPORT No. 4/1980

HIGH-RESOLUTION STUDY OF E0 INTERNAL-PAIR TRANSITIONS FROM EXCITED 0^+ STATES IN $^{58, 60, 62}$Ni

BY
ARTO PASSOJA

Academic dissertation
for the Degree of
Doctor of Philosophy

To be presented, by permission of the
Faculty of Mathematics and Natural Sciences
of the University of Jyväskylä,
for public examination in Auditorium II-212 of the
University of May 14, 1980, at 12 o'clock noon.

Jyväskylä, Finland
April 1980

Preface

The work presented in this thesis has been carried out during the years 1977-79 at the Department of Physics, University of Jyväskylä. I wish to express my sincere thanks to this institute for providing the excellent working conditions.

I am indebted to numerous people for their assistance in the course of this work. Special appreciation is extended to my teacher, Professor J. Kantele. He initiated the EO project and offered a wealth of ideas for the special techniques needed, including the topic of this thesis. His continuous interest and encouragement throughout the course of this work have been of great value.

To my coworkers, Dr. R. Julin and Mr. M. Luontama, M.Sc., I am greatly indebted for enjoyable co-operation. I also want to extend my thanks to the staffs of the cyclotron, the target laboratory and the machine shop at JYFL for their valuable assistance in my countless, necessary but often thankless, tasks. The successful efforts of Mr. T. Komppa, Lic. Phil., at adapting the various data-handling procedures to computer operation are gratefully acknowledged. I wish to thank all my colleagues as well.

I am indebted to Professor P.O. Lipas for revising the language of the manuscript. My thanks also go to Miss T. Tuominen, who carefully typed this thesis, and to Mr. T. Näränen, who skillfully finished the drawings.

Furthermore, I wish to thank my wife for her support and understanding throughout the work. The continuous encouragement of my parents is also gratefully acknowledged.

This work is supported by grants from the Emil Aaltonen Foundation, the Leo and Regina Wainstein Foundation, the Jenny and Antti Wihuri Foundation and the Oskar Öflund Foundation, and by travel grants from the Academy of Finland, the Finnish Cultural Foundation, the Magnus Ehrnrooth Foundation, the Alfred Kordelin Foundation and the University of Jyväskylä, for which I wish to express my gratitude.

Jyväskylä, April 1980

Arto Passoja

HIGH-RESOLUTION STUDY OF EO INTERNAL-PAIR TRANSITIONS FROM EXCITED 0^+ STATES IN $^{58,60,62}Ni$

Abstract

A new method based on a combination of an intermediate-image magnetic lens and two cooled Si(Li) detectors has been developed for in-beam studies of internal-pair transitions. Calculations of the spectrometer pair-line efficiency for EO, El, E2 and Ml transitions versus transition energy are made in the zero-order Born approximation. The main advantages gained over the previous methods used for pair-line measurements are an excellent energy resolution of the sum-coincidence pair lines (4-6 keV) and a high pair-line efficiency ($\approx 10^{-3}$) provided by the high transmission and the broad momentum band width of the magnetic lens. With the aid of the new technique the first extensive systematic investigation of the EO transitions has been carried out in $^{58,60,62}Ni$. The present internal-pair measurements confirmed the 0_3^+ assignment of the 3530.9 keV state in ^{58}Ni and the 3318.3 keV state in ^{60}Ni, and yielded a spin and parity assignment of 0_4^+ for the 3588.0 keV state in ^{60}Ni. The X(EO/E2) values are determined for these states and for the 0_2^+ states at 2942.3 keV, 2284.8 keV and 2048.4 keV in ^{58}Ni, ^{60}Ni and ^{62}Ni, respectively. The results are combined with the available lifetimes of these states to extract the monopole strengths $\rho^2(0_i^+ \rightarrow 0_1^+)$. The results and the nature of the 0^+ states are discussed.

Contents

Errata

Page 6, line 7 from bottom, in equation: $|0_1^+>$ should read $|0_i^+>$

Page 6, line 7 from bottom, equation number (3) should be omitted

Page 8, line 1, $\left[\frac{\quad}{\quad}\right]$ should read $\left[\frac{\quad}{\quad}\right]$

Page 19, line 10, "constructed" should read "connected"

Page 28, line 9 from bottom, "distrortion" should read "distortion"
Page 38, line 8 from bottom, "... is an axis of ..." should read "... is the axis of ..."

Page 47, line 9, "consist to" should read "consist of"

Page 66, table 4, $T_{1/2}(0_4^+) < 40$ ps [b] should read $T_{1/2}(0_4^+) < 40$ ps [c]

Page 74, line 9, "... for which $^2_{vibr}$ ..." should read "... for which ρ^2_{vibr} ..."

Page 77, line 13, "coincidence" should read "coincidences"

Page 78, line 4 from bottom, "... would be be the ..." should read "... would be the ..."

Page 79, line 3, "wprk" should read "work"

Page 84, ref. 22, "nad" should read "and"

Page 85, ref. 30, "Gl Wilhelmi" should read "G. Wilhelmi"

1. INTRODUCTION

Since 1975 a project aimed at systematic studies of excited 0^+ states and especially their E0 and E2 decay properties has been carried out at the Cyclotron Laboratory of the University of Jyväskylä, partly in collaboration with other laboratories[1-8]. In connection with this project electron spectrometers[1,2] of two types have been constructed; special attention has been paid to direct lifetime-measurement and coincidence methods based on the use of the natural pulsing of the cyclotron[3,4].

The main research subjects of the project have been the regions of the closed nuclear shells. A natural extension of our previous experiments around doubly magic $^{208}_{82}Pb_{126}$ (ref. 5), in the Sn region[6,7] (Z = 50 closure) and most recently on doubly magic $^{146}_{64}Gd_{82}$ (ref. 8), when going to lower Z, would be the region around doubly magic $^{56}_{28}Ni_{28}$ in the f-p shell. The excitations and the level structure of the nickel isotopes are of considerable interest for nuclear-structure calculations. The closure of the $f_{7/2}$ shell at ^{56}Ni leads to a simple shell-model description of the low-lying states with the proton shells completely inert and the valence neutrons in the $2p_{3/2}$, $2p_{1/2}$ and $1f_{5/2}$ orbitals[9-12].

The energies of excited 0^+ states and the principal channels of their de-excitation, electric quadrupole E2($0^+ \rightarrow 2^+$), magnetic dipole M1($0^+ \rightarrow 1^+$) and electric monopole E0($0^+ \rightarrow 0^+$) transitions, are of critical importance in determining the applicability to nickel isotopes of different nuclear models. E0 transitions are related to the change in the mean square radius between the initial and final states of a nucleus and thus are sensitive to the details of nuclear structure.

Experimental data on the energies and decay properties of the excited 0^+ states in even-even nuclei have been reviewed in ref. 13. It is found that electric monopole transitions have been studied in several medium-weight nuclei. However, the measurements of E0 transition rates in nickel isotopes are missing, except for the case of the 0_2^+ state in ^{58}Ni (ref. 14). The lack of experimental data on E0 branching ratios in ^{58,60,62}Ni is due to difficulties in detecting E0 transitions of 2-4 MeV energy, which proceed predominantly via internal pair formation (π; IPF).

E0 internal-pair decay branches of the order of $< 10^{-3}$ and the fairly high level density in nickel isotopes demand for E0 measurements a high-resolution pair spectrometer that collects the electron-positron pairs with high efficiency. All previous methods developed for in-beam studies of internal-pair transitions have limitations associated with the pair-line efficiency; an increase of the efficiency has always led to a poor pair-line resolution (subsect. 3.3.1).

In the present work a new method for high-resolution in-beam studies of internal pair transitions has been developed[15,16]. The method is based on the use of an intermediate-image magnetic spectrometer and cooled Si(Li) detector(s): the electron and the positron spiral, along the axial magnetic field, from the target to the detector(s) simultaneously, the sense of rotation being of opposite sign. The energies of the particles are summed in a single Si(Li) detector, or a Si(Li)-Si(Li) sum-coincidence technique is used.

The first part of this thesis consists of a short presentation of the characteristics of the de-excitation of 0^+ states. The experimental methods employed, especially the new method for high-resolution pair-line measurements, are described in chap. 3.

In chap. 4 the experiments involved in the measurements of E0, M1 and E2 decay branching ratios from excited 0^+ states in ^{58,60,62}Ni are presented. (i) The new pair spectrometer is employed to measure E0 internal-pair decay branches. (ii) In studies of M1 and E2 transitions, singles conversion-electron spectra, anti-Compton gamma-ray spectra and γp coincidence spectra are recorded. Finally, the results are discussed in terms of theoretical models in sect. 4.4.

Most of the experimental methods and results presented in this thesis have been included in the following publications (1-3) and reports (4-5):

1. A. Passoja, J. Kantele, M. Luontama and R. Julin:
A method for high-resolution in-beam studies of internal pair transitions
Nucl. Instr. and Meth. 157 (1978) 513
https://doi.org/10.1016/0029-554X(78)90011-3

2. M. Luontama, J. Kantele, R. Julin, A. Passoja, T. Poikolainen and M. Pylvänäinen:
A combination intermediate-image magnetic plus Si(Li) electron spectrometer for in-beam experiments
Nucl. Instr. and Meth. 159 (1979) 339
https://doi.org/10.1016/0029-554X(79)90659-1

3. A. Passoja, J. Kantele, R. Julin and M. Luontama:
A combination magnetic plus Si(Li)-Si(Li) sum-coincidence technique for in-beam studies of internal pair transitions
Nucl. Instr. and Meth. 166 (1979) 203
https://doi.org/10.1016/0029-554X(79)90575-5

4. A. Passoja, J. Kantele and M. Luontama:
Present status of the JYFL internal-pair spectrometer project
JYFL Annual Report 1979, 1.4

5. A. Passoja, R. Julin, J. Kantele and M. Luontama:
Electromagnetic decay of excited 0^+ states in ^{58,60,62}Ni
JYFL Annual Report 1979, 3.2, and to be published

2. CHARACTERISTICS OF DE-EXCITATIONS OF 0^+ STATES

2.1. Probability of E0 transition

Single-photon nuclear transitions between 0^+ states are forbidden by the law of conservation of angular momentum. In this case a radiative transition occurs by emission of two (or more) quanta. The cause of E0 transitions is the Coulomb interaction between the nucleons and the electrons of the atomic shell or the Dirac background; the most probable processes are the emission of one internal-conversion electron or an electron-positron pair, respectively. The latter process is energetically allowed when the transition energy is larger than twice the electron rest mass.

E0 conversion differs substantially from other multipole conversion processes in that the Coulomb interaction which causes these transitions takes place inside the nucleus (since the monopole moment is constant outside the nuclear volume), while in other conversion processes the region of the nucleus makes a relatively small contribution. Calculations of monopole conversion probability must therefore allow for the finite size of the nucleus. For a point nucleus, an E0 conversion transition is strictly forbidden.

The total E0 transition probability, neglecting two-photon and many-particle emissions, can be written in the form

$$W(E0) \equiv W_e(E0) + W_\pi(E0) = \frac{1}{\tau(E0)} ,$$

where $\tau(E0)$ is the lifetime of the excited nucleus corresponding to the E0 transition, W_e is the total probability of electron conversion

from different atomic shells, and W_τ is the probability of internal pair formation.

The partial electric monopole transition probabilities $W_{K,\pi}(EO)$ can be written[17] as a product of an electronic factor $\Omega(EO)$ and a monopole strength $\rho^2(EO)$ which contains all nuclear information:

$$W_{K,\pi}(EO;\ 0_i^+ \to 0_f^+) = \rho^2(0_i^+ \to 0_f^+) \cdot \Omega_{K,\pi}(Z,k) .$$

The electronic factors $\Omega_{K,\pi}(Z,k)$ are associated with the electron transition probability from the K shell to the continuum state or with the formation of an electron-positron pair. These factors $\Omega_{K,\pi}(Z,k)$ can be precisely calculated from Dirac's relativistic electron theory. Numerical calculations of the factors $\Omega_{K,\pi}(Z,k)$ are discussed in more detail in sect. 2.2.

The monopole strength parameter ρ, on the other hand, is related to the transition probability between the 0^+ states of the nucleus and is obtained for an $EO(0_i^+ \to 0_f^+)$ transition in the form[17]

$$\rho(EO;\ 0_i^+ \to 0_f^+) = \langle 0_f^+ | \sum_j e_j r_j^2 | 0_i^+ \rangle / eR_0^2 , \qquad (3)$$

where R_0 is the nuclear radius ($1.20\ A^{1/3}$ fm) and where the monopole operator in the matrix element is taken as a sum over the charged particles in the nucleus.

The experimental monopole strength for an $EO(0_i^+ \to 0_f^+)$ transition is often obtained by means of the branching ratio of the cascade E2 and crossover E0 transitions:

$$\rho^2(E0;0_i^+ \to 0_f^+) = \frac{I_{K,\pi}(E0;0_i^+ \to 0_f^+)}{\Omega_{K,\pi}(E0;0_i^+ \to 0_f^+)} \times \frac{\alpha_{K,\pi}(E2;0_i^+ \to 2_j^+)}{I_{K,\pi}(E2;0_i^+ \to 2_j^+)} \times W_\gamma(E2;0_i^+ \to 2_j^+) \ ,$$

where $I_K(EL;I_i \to I_f)$ is the observed K conversion-electron intensity and $I_\pi(EL;\ I_i \to I_f)$ the internal-pair intensity in the EL transition between the spin I_i and I_f states, and $\alpha_{K,\pi}(E2)$ is the E2 (K electron or internal pair) conversion coefficient. The absolute E2 transition probability $W_\gamma(E2)$ can be written as

$$W_\gamma(E2;0_i^+ \to 2_j^+) = 0.0122 \cdot E_\gamma^5(E2) \cdot B(E2;0_i^+ \to 2_j^+) \ ,$$

where B(E2) is the reduced E2 transition probability in units of e^2b^2,

$$B(E2;0_i^+ \to 2_j^+) = 56.4 \cdot \left\{T_{1/2}(E2)\ E_\gamma^5(E2)\right\}^{-1}\ e^2b^2,$$

and $E_\gamma(E2)$ is given in keV.

If the absolute transition probabilities cannot be determined, the experimental ratio of reduced transition probabilities of competing E0 and E2 transitions de-exciting the 0^+ state is usually reported as

$$X\left(\frac{E0;0_i^+ \to 0_j^+}{E2;0_i^+ \to 2_j^+}\right) = \frac{B(E0;0_i^+ \to 0_f^+)}{B(E2;0_i^+ \to 2_j^+)} \ ,$$

where $B(E0;0_i^+ \to 0_f^+) = e^2R_0^4\rho^2(0_i^+ \to 0_f^+)$ is the reduced E0 transition probability. The experimental ratio X(E0/E2) is determined from the relative E0 and E2 conversion (electron or internal pair) intensities as follows:

$$X\left[\frac{E0;0_i^+ \to 0_f^+)}{E2;0_i^+ \to 2_j^+)}\right] = 2.56\cdot 10^{-6}\, A^{4/3}\, \frac{E_\gamma^5(E2)\cdot\alpha_{K,\pi}(E2)}{I_{K,\pi}(E2)} \cdot \frac{I_{K,\pi}(E0)}{\Omega_{K,\pi}(E0)}\,,$$

where $E_\gamma(E2)$ is given in keV.

2.2. Competition of IPF and IC in E0 transitions

The electronic factor $\Omega_\pi(E0)$ depends on the form of the wave functions belonging to the continuous spectrum of both positive and negative electron levels. Dalitz has calculated an expression for $W_\pi^{Z=0}(E0)$ in the Born approximation[18]. Wilkinson[19] extended this result by taking the nuclear Coulomb effects into account. Numerical calculations of $\Omega_\pi(E0)$ given by Lombard et al.[21] are limited to transition energies (in units of electron rest mass) $k \leq 5$. In the present work the electronic factor $\Omega_\pi(E0)$ has been computed[20] for $20 \leq Z \leq 50$ and $2.5 \leq k \leq 16$ on the basis of refs. 18 and 19. Fig. 1 shows graphically the dependence of $\Omega_\pi(E0)$ on the atomic number Z and the transition energy k.

The electronic factor $\Omega_K(E0)$ for the K shell has been given by Church and Weneser[17] in a "point-nucleus" approximation (using Coulomb state functions of a point nucleus evaluated at the actual nuclear radius $R_0 = 1.20\ A^{1/3}$ fm). Numerical calculations of $\Omega_K(E0)$ have been given by Hager and Seltzer[22] for atomic numbers $Z \geq 30$ and transition energies $E \leq 1500$ keV and by Bell et al.[23] for $Z \geq 40$ and $E \leq 2500$ keV. No numerical calculations are available for $Z = 28$ and transition energies from 2000 to 4000 keV.

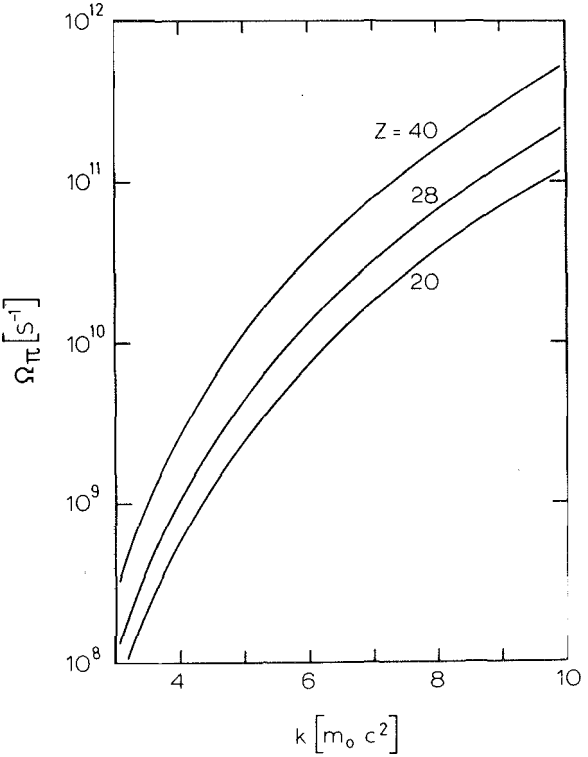

Fig. 1. The electronic factor $\Omega_\pi(E0) = W_\pi(E0)/\rho^2(E0)$ for internal pair formation as a function of transition energy k and atomic number Z.

In the present work the electronic factor $\Omega_K(E0)$ has been computed[20] for $20 \leq Z \leq 50$ and $0.1 \leq k \leq 12$ on the basis of refs. 17 and 23. Fig. 2 shows graphically the dependence of $\Omega_K(E0)$ on Z and k.

The corrections to $\Omega_K(E0)$ due to finite nuclear size and bound-state atomic screening are not included in the present calculations. A comparison of the present $\Omega_K(E0)$ values with those of Hager and Seltzer[22] and of Bell et al.[23], which include corrections for these effects, is given in appendix I. It turns out that for $Z \leq 40$ and $k \geq 1$ the influence of these corrections is negligible, typically less than 2 %.

In the present work the ratio of internal pair formation to internal K conversion has been computed[20] for $20 \leq Z \leq 48$ and $3 \leq k \leq 12$. The curves for $\Omega_\pi(E0)/\Omega_K(E0) = W_\pi(E0)/W_K(E0)$ as a function of transition energy k and atomic number Z are shown in fig. 3. It is observed from fig. 3 that, e.g., for Z = 28 the ratio $W_\pi(E0)/K_W(E0)$ is 10 and 50 at transition energies 2.40 MeV and 3.46 MeV, respectively. This ratio is important for the evaluation of E0 transition measurements; in E0 transitions in the nickel isotopes internal pair formation is the dominating decay channel.

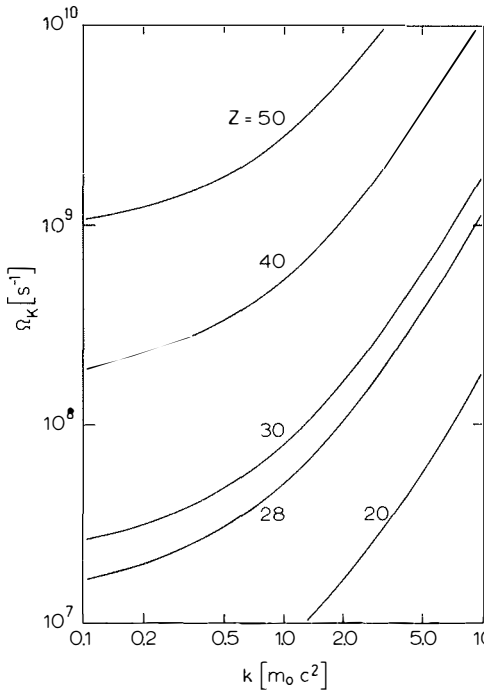

Fig. 2. The electronic factor $\Omega_K(E0) = W_K(E0)/\rho^2(E0)$ for electron conversion in the K shell as a function of transition energy k and atomic number Z

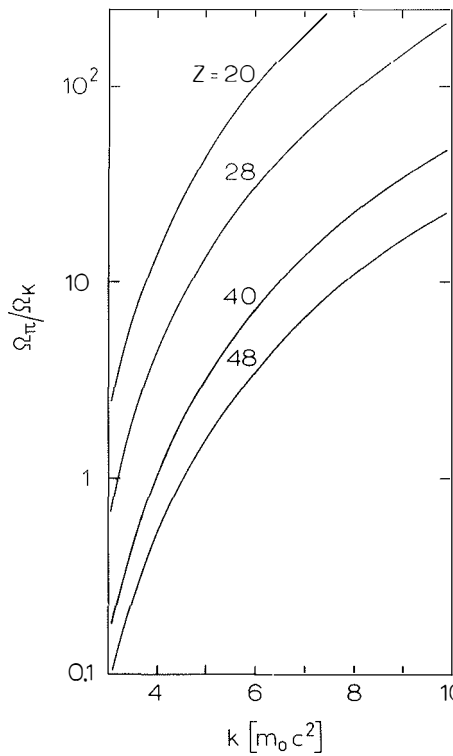

Fig. 3. The ratio of internal pair formation to internal K conversion for electric monopole transitions as a function of transition energy k and atomic number Z

2.3. Angular correlation of internal pairs

The emission of internal pairs, referred to the total number of transitions, is described[24-27] by the angular correlation function $F_\ell(\Theta,\delta,\theta_q,\phi_q,W_+)$, where Θ is the angle between the positron and electron momenta, $\vec{p}_+$ and $\vec{p}_-$, θ_q and ϕ_q are the polar and azimuthal angles of $\vec{q} = \vec{p}_+ + \vec{p}_-$, and δ is the dihedral angle formed by the planes $(\vec{z},\vec{q})$ and $(\vec{p}_+,\vec{p}_-)$, where z is a vector in the direction of the axis of quantization (beam axis) and $W_\pm$ refer to the total energy of the positron and electron ($W_+ + W_- = k$, in units of m_0c^2). The angles associated with $\vec{q}$ are shown in fig. 4.

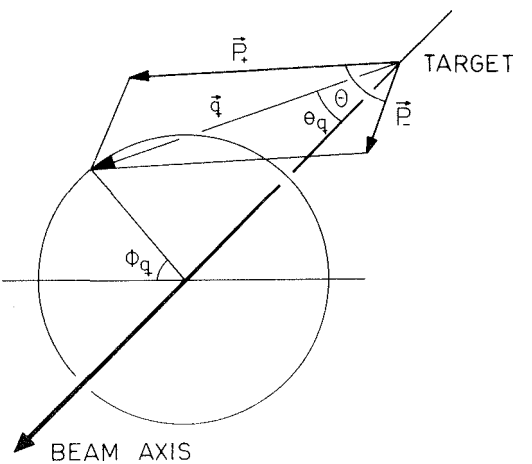

Fig. 4. The angles Θ, θ_q and ϕ_q associated with $\vec{q} = \vec{p}_+ + \vec{p}_-$

For pure multipoles and nonaligned nuclei[27]

$$8\pi^2 F_\ell(\Theta,\delta,\theta_q,\phi_q,W_+) = \gamma_\ell(\Theta,W_+),$$

which is the differential internal-pair-formation coefficient integrated over all angles except Θ, the energies $W_\pm$ being fixed. The $\gamma_\ell(\Theta,W_+)$ functions are obtained from the Born approximation results of Oppenheimer for EO transitions[28] and of Rose for other electric and magnetic multipoles[24,25] and are given explicitly in appendix II.

The angular correlation of internal pairs is very important for the design of an internal-pair spectrometer. One may ask, for example: is one magnetic channel more effective for collecting pair components than two magnetic channels used in opposite directions? This question was answered by calculating the angular-correlation curves starting from the condition of the JYFL intermediate-image plus Si(Li) combination electron spectrometer[2] that the mean acceptance angle of the spectrometer is $\alpha \approx 50^o$. The results are given in figs. 5a and b for the special case of $W_+ = W_-$. The azimuthal angle ϕ between the pair components is used instead of the separation angle Θ at the moment of emission ($\cos^2 \frac{1}{2}\Theta = 1 - \sin^2\alpha \sin^2 \frac{1}{2}\phi$.

From fig. 5a it is found that the electron-positron pairs are preferentially emitted with small angular separation. Fig. 5b shows that this behaviour still increases for higher multipoles when increasing the transition energy. For EO transitions the ratio $\gamma_{EO}(\phi)/\gamma_{EO}(0^o)$ is energy independent.

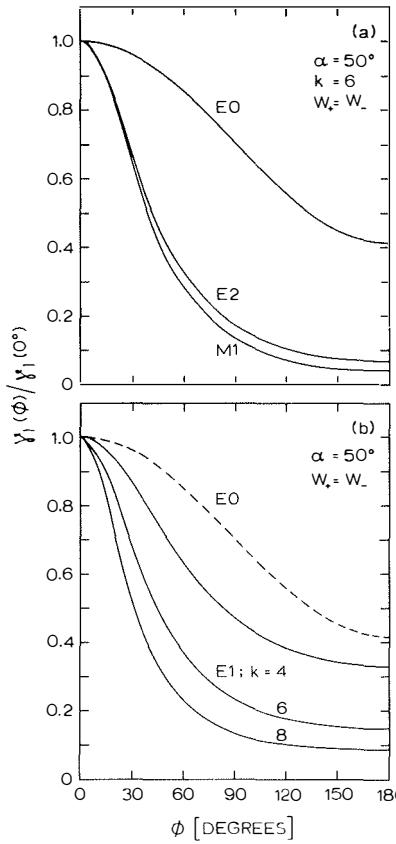

Fig. 5. The angular correlation of electron-positron pairs for the special case of equal energy division between the pair components and the spectrometer mean acceptance angle $\alpha = 50^{o}$: (a) the angular correlation in E0, M1 and E2 transitions for 3 MeV transition energies, and (b) in E1 transitions for various transition energies; the ratio $\gamma_{E0}(\phi)/\gamma_{E0}(0^{o})$ (energy independent) is sketched in the figure by a dashed curve.

In summary, it is concluded that the design of a pair spectrometer which collects electron-positron pairs with a high efficiency has to take into account internal pairs emitted with small azimuthal angle ϕ between the pair components. One magnetic channel featuring a large solid angle and a broad momentum band width offers optimized conditions for collecting the pair components and the use of semiconductor detectors to produce the energy sum leads to measurements of high-resolution pair-line spectra.

The pair-line efficiency (sect. 3.3.5.) depends to some extent on the angular correlation of the electron-positron pair, which in turn depends on the transition multipolarity (fig. 5). The measurement of the relative pair-line efficiencies has proved[29-31] to be an effective method of determining multipolarities of high-energy transitions. An intermediate-image magnetic pair spectrometer can be modified to respond to positron-electron pairs emitted at large relative angles ($60^{o} \leq \theta \leq 100^{o}$) using (i) a specially designed baffle system[29] or (ii) a special detector geometry. The latter method is a new idea which has not been tested yet. The differential probabilities for production of pairs with large angular separation depends critically upon the multipole order. Fig. 5 shows that a multipole meter, based on large relative angles θ, can alone give a definite assignment of an E0 transition. The strong similarity of M1, E1 and E2 curves means that extra supporting information is needed for definite multipole assignments of these transitions.

3. EXPERIMENTAL METHODS

3.1. Gamma-ray spectrometry

In most measurements of gamma-ray spectra a coaxial Ge(Li) detector with an active volume of 42 cm^3 was employed. The energy resolution of the Ge(Li) detector was typically 2.5 keV at 1.33 MeV. In the case of nickel isotopes the Doppler effect usually determines the width of the gamma-ray lines.

Anti-Compton gamma-ray measurements were carried out in order to decrease the Compton background under the low-lying weak gamma-ray lines and to reduce the single and double escape peaks in the high-energy part of the gamma-ray spectra. Both singles and anti-Compton gamma-ray spectra were measured at 125^o with respect to the beam.

In the gamma-proton coincidence measurements the gamma-ray spectra were recorded at 90^o to the beam. A 110 mm^2 × 3 mm Si(Li) detector was used as the particle detector. The Si(Li) detector was placed at back angles (≈ 135^o), and the distance from the target was varied from 10 to 30 mm. Fig. 6 shows a singles particle spectrum from the $^{58}Ni(p,p')$ reaction at E_p = 6.9 MeV measured with a target-to-detector distance of 30 mm.

Energy calibration of the gamma-ray spectra was performed mainly by means of internal calibration using the adopted gamma-ray energies of refs. 32-35. Efficiency calibration of the Ge(Li) detectors was carried out with ^{133}Ba, ^{152}Eu and RdTh sources.

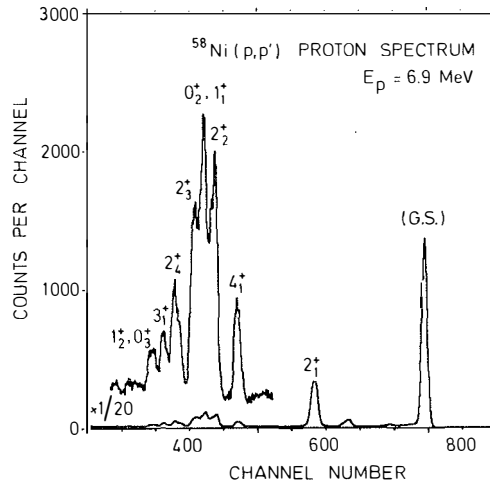

Fig. 6. Singles proton spectrum from the ^{58}Ni(p,p') reaction at E_p = 6.9 MeV. The peaks are labelled by the ^{58}Ni levels populated. The target thickness was 0.8 mg/cm^2, the target - to - particle-detector distance 30 mm at ≈ 135^o and the overall energy resolution ≈ 80 keV.

3.2. Magnetic plus Si(Li) electron spectrometer

3.2.1. Construction

In connection with the project for systematic study of electric monopole transitions, two types of electron spectrometer have been designed in Jyväskylä[1-2]. In this work the intermediate-image magnetic plus Si(Li) spectrometer[2] has been employed as a conventional in-beam electron spectrometer, and after removal of baffles designed to stop positrons as an in-beam pair spectrometer (sect. 3.3).

The electron-spectrometer construction is based on two identical lenses of the type designed by Kleinheinz et al.[36], constructed together by an aluminium collar covered by soft iron. The details of the construction of the spectrometer are shown in fig. 7. The magnet part of the spectrometer has twelve water-cooled coil sections. In most runs, the current is passed only through the eight outermost coils of the system, which thus may be called the 4+4 coil configuration. With this configuration, the field form is very similar to that of an intermediate-image beta spectrometer.

The beam enters the spectrometer axially, which is advantageous from the point of view of the symmetry of the acceptance angles (which allows accurate ICC determinations and IPF measurements). The beam is stopped in a Faraday cup made of lead.

In singles spectrum measurements, the magnet current is swept with a triangular wave form of a period of about 1 min. The current sweeping range and the settings needed in fixed-current runs can be selected quickly with the aid of helipot controls. The electron spectra are recorded with a cooled Si(Li) detector.

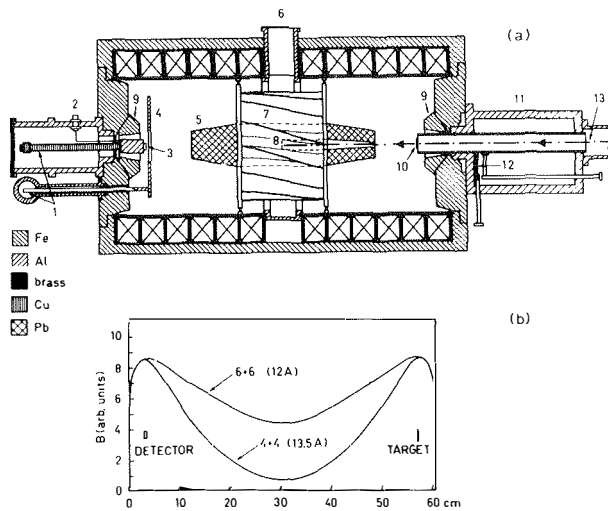

Fig. 7. (a) Schematic cross-sectional diagram of the intermediate-image + Si(Li) electron-spectrometer configuration: (1) cold fingers, (2) to preamplifier, (3) Si(Li) electron detector, (4) cold trap, (5) lead shield, (6) to pump, (7) anti-positron baffle, (8) Faraday cup, (9) extra iron pieces, (10) target/source, (11) target/source changing system, (12) gate valve, (13) beam (collimators not shown). (b) Magnetic field distribution along the lens axis for the 4+4 and 6+6 coil configurations. The positions of the target and the detector indicated correspond to the 4+4 configuration.

A 110 cm^2 by 3 mm thick Kevex Si(Li) detector with a cooled FET preamplifier was used in most of the conversion-electron measurements. The energy resolution of the 110 mm^2 Si(Li) detector is about 1.3 keV at 320 keV and about 2.3 keV at 975 keV. In a typical in-beam run the target thickness and, e.g. in the case of nickel isotopes, the Doppler effect determine the width of the conversion lines.

Energy calibration of the electron spectrometer was performed by means of an internal calibration or with ^{133}Ba, ^{207}Bi and ^{152}Eu sources. Detector efficiency $\varepsilon_d(k)$ was determined with the former sources, and in the case of high-energy conversion lines (1.7-2.4 MeV) with the aid of theoretical E2 conversion coefficients or with sources of continuous beta spectra. The relative efficiency curve obtained is believed to be accurate to better than ± 10 % for transition energies smaller than 1.7 MeV and about 15 % for transition energies of 1.7-2.3 MeV.

3.2.2. Transmission and efficiency

For the most often used coil configuration (4+4), the average angle of acceptance of the spectrometer is $\alpha \approx 50^o$, which corresponds to $P_2(\cos \alpha) \approx P_2(\cos 55^o) = 0$. For that reason problems associated with angular distributions and particle parameters are diminished. A comparison of the electron spectrum with the corresponding gamma-ray spectrum taken at $\alpha = 55^o$ or 125^o yields internal-conversion coefficients with good accuracy.

When the fixed current mode of operation is used, the overall efficiency of the spectrometer $\varepsilon_e(k)$ is defined as the ratio of the total absorption-peak count rate to the emission rate of electrons with the corresponding energy from the source. It is equal to the effective transmission tf_d multiplied by the detector efficiency $\varepsilon_d(k)$.

The transmission t represents the percentage of the monokinetic electrons emitted within 4π which would reach the image plane and form

the image in a case where emission was isotropic. The acceptance factor f_d measures the ratio between the electrons accepted by a given detector window and the electrons transmitted to the image position. This parameter is ≤ 1 and is important because Si(Li) detectors of various sizes (80-300 mm^2) are used and are typically smaller than the image.

The intrinsic efficiency of a Si(Li) detector $\varepsilon_d(k)$ depends on the angle at which the electron enters its surface and on the electron energy. For perpendicular entry the efficiency is highest ($\varepsilon_d \approx 0.85$) and decreases with increasing angle between the electron path and the normal of the detector surface[2,37]. The detector efficiency $\varepsilon_d(k)$ for the 110 mm^2 detector at energies up to about 1.5 MeV is approximately 0.60 in the present spectrometer ($\alpha \approx 50^o$).

The overall efficiency of the spectrometer $\varepsilon_e(k) = t\, f_d\, \varepsilon_d(k)$ was measured for the different coil configurations using a calibrated ^{207}Bi source and a 110 mm^2 by 3 mm thick Si(Li) detector. Table 1 lists some typical overall efficiencies, momentum band widths and relative sweeping-mode efficiencies[1] measured without the anti-positron baffle. The maximum energies measurable with the different configurations are also given.

A slightly greater acceptance factor could be obtained with a larger detector diameter. To test this possibility a Si(Li) detector having an area of 200 mm^2 was employed. With the 4+4 coil configuration an overall efficiency of 10.6 % was measured. For singles conversion-electron experiments the gain in efficiency from 7.5 % to 10.6 % is perhaps not significant. However, for internal-pair-formation measurements, to be discussed in the next section, this gain means a factor of 2 in pair-line efficiency.

Table 1

Overall efficiency ε_e, momentum band width $\Delta p/p$ and relative sweeping-mode efficiency ε_{rel} for some coil combinations, as measured for 975 keV electrons using a 110 mm^2 by 3 mm thick Si(Li) detector (no anti-positron baffles in the lens). The maximum measurable energies E_{max} are also given.

Coil combination	ε_e (%)	$\Delta p/p$ (%)	ε_{rel}	E_{max} (MeV)
4 + 4	7.5	24	4	2.2
5 + 5	5.2	17	2	3.0
6 + 6	3.5	12	1	3.8

In singles in-beam conversion-electron spectrometry, a high swept-current-mode efficiency is obtained, owing to the large $\varepsilon_e(k)$ and $\Delta p/p$ values of the system. Studies of internal pair transitions are possible with this spectrometer owing to the same reasons.

3.3. New method for high-resolution IPF measurements

3.3.1. Introduction

Many magnetic beta-ray spectrometers have been used for measurements of internal pair formation[38-42]. With the aid of an intermediate-image spectrometer and a statistical-separation detector[41,42], a pair-line efficiency of 10^{-4} has been achieved at the maximum transmission settings. Under such conditions, the pair-line width is 2.5 % in momentum, corresponding to a 7 % transmission of the magnetic lens. A typically used resolution of 1.3 % corresponds to a pair-line efficiency of only 5×10^{-6}.

A high pair-line efficiency ($2\text{-}5 \times 10^{-2}$) has been achieved using two double-coincidence scintillation telescopes[43,44]. The very poor energy resolution of the scintillation spectrometer has been compensated for by using an annular counter (Ω = 0.10 sr), operated in coincidence with the spectrometer, to detect particles feeding the excited state through (particle,particle) nuclear reactions. The use of this type of spectrometer is limited to cases in which a very poor energy resolution is sufficient.

A pair spectrometer which is based on the resolution, sensitivity and coincidence capabilities of semiconductor detectors has been proposed by Michaelis and Lange[30,45]. The main components of the spectrometer are a simple (dE/dx + E)-type silicon detector telescope and two NaI(Tl) scintillation counters operated in a fourfold coincidence. A large solid angle is provided by the use of a superconducting magnet. In the case of a homogeneous field of sufficient strength, almost 50 % of all pairs leaving the target will reach

the telescope with an optimum resolution of 0.07 %. No actual in-beam applications of this method appear to have been reported.

In the case of a magnetic pair spectrometer, the pair-line efficiency obviously strongly depends on both the transmission and the momentum band width of the magnetic lens. A high efficiency is possible only if both are large. During the past several years, several magnetic plus Si(Li) combination electron spectrometers have been constructed. However, most of them cannot be used in internal-pair studies, owing to transmission and momentum-band-width limitations.

In the present work, the intermediate-image magnetic plus Si(Li) combination spectrometer, described in sect. 3.2., featuring high transmission and momentum band width has been adapted to internal-pair-formation measurements[15-16]. An excellent energy resolution is obtained with the aid of cooled, high-resolution Si(Li) detector(s), and also the detection efficiency is greatly improved as compared to the previous magnetic pair spectrometers. The present spectrometer is especially intended and suited for the study of EO transitions.

3.3.2. Operating principle

The operating principle of the internal-pair spectrometer is demonstrated in figs. 8a and b using the 4+4 coil configuration (no anti-positron baffles in the lens). The $^{90}Zr(p,p')$ reaction at E_p = 6.9 MeV was employed to populate the first excited 1762 keV 0_2^+ state in ^{90}Zr with a total cross section[46] of 11 mb. The target was a self-supporting natural-Zr-metal foil of 0.8 mg/cm^2 thickness. The 0_2^+ state decays only via an E0 transition to the ground state, the experimental K/π ratio[47] being 2.08(8). Fig. 8a shows the energy range of 0.1-2.0 MeV recorded using the sweeping mode of operation. The E0 conversion-electron lines and the continuous energy spectra of electrons and positrons superimposed on each other are observed. At the magnetic field setting corresponding to the energy of $\frac{1}{2} \times (1762 - 1022)$ keV, both pair components (the electron and the positron) of the E0 transition can spiral from the target to the detector simultaneously, provided that they satisfy the acceptance-angle and momentum-window conditions, the sense of rotation being of opposite sign. In fig. 8b are shown the fixed momentum window at 370 keV and the 1762 keV pair line, which can also be seen in fig. 8a at the end-point energy of the continuous electron and positron spectra. The pair-line resolution achieved is 3.2 keV.

The total emission of E0 pairs in the above experiment was determined using the observed K conversion-line intensity and the experimental value for ^{90}Zr K/π branching ratio[47]. The experimental value of the pair-line efficiency ε_{E0}^{π}(1762 keV), defined as the ratio of the observed pair counting rate to the total emission rate of pairs

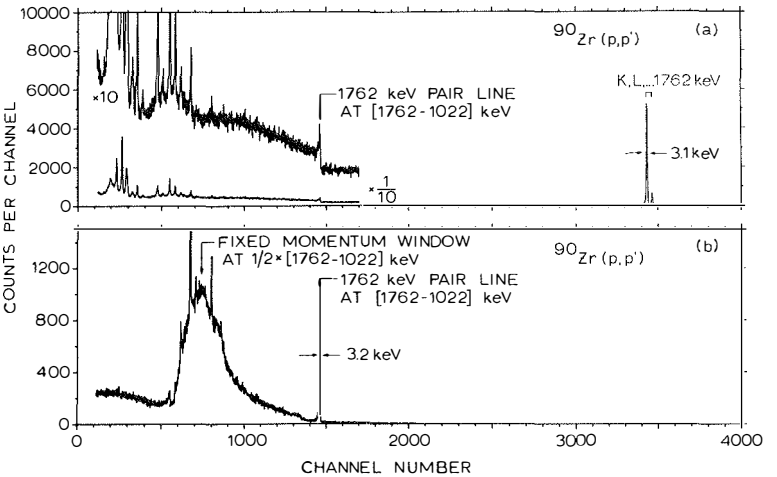

Fig. 8. Internal pair line from the decay of the ^{90}Zr (1762 keV, 0_2^+) state, populated in the ^{90}Zr(p,p') reaction at E_p = 6.9 MeV, obtained with the combination intermediate-image magnetic plus Si(Li) pair spectrometer in different modes of operation: (a) the energy range 0.1-2 MeV recorded using the sweeping mode of operation. The pair-line can be seen at the end-point energy of the continuous electron and positron spectra. (The low-energy conversion lines observed are not relevant.) (b) the 1762 keV pair-line obtained using a fixed momentum window at 370 keV. The pair energy resolution is 3.2 keV.

belonging to the same transition, is $(1.18 \pm 0.10) \times 10^{-3}$ for a 110 mm^2 by 3 mm thick Si(Li) detector and for the 4+4 coil configuration.

3.3.3. Background contributions and reduction

Owing to the fact that the direct spectrum of the silicon detector is recorded, disturbing background counts of several kinds are found under the pair line: (a) scattered high-energy electrons and positrons, (b) pulse pile-up counts, (c) continuum pairs, (d) counts due to neutrons and gamma rays. Since the internal-pair-formation coefficient is typically about 10^{-4} to 10^{-3} and the pair-line efficiency about 10^{-3}, the background can seriously limit the usefulness of a combination magnetic plus semiconductor pair spectrometer in the observation of weak pair lines. It should be pointed out that the ^{90}Zr 1762 keV transition demonstrated in subsect. 3.3.2. represents a favourable case, since the E0 transition observed is fairly intense and the background radiations are weak.

The main counting rate of the Si(Li) detector is caused by electrons having an energy corresponding to the open momentum window. The occurrence of two unrelated events within the resolving time of the energy-channel amplifier results in a piled-up signal and causes a disturbing background. A pile-up inspector is used to provide an inhibit output to reject the piled-up signal in a linear gate following the energy amplifier. Spectral distrortion caused by pulse pile-up can be reduced typically by a factor of 10-15.

However, if no coincidence device is available, the background may disturb the pair-line measurements, e.g. in the presence of strong β^+ activity as will be demonstrated in subsect. 3.3.4. In order to make the pair spectrometer more universally applicable, further work was carried out for reducing the background under the pair lines. Among others, the following coincidence methods were tested for background rejection:

(i) The use of a (dE/dx + E)-type silicon detector telescope[30,45,48] is demonstrated in fig. 9, which shows pair spectra from the decay of the lowest excited $^{12}C(4.43\ MeV;\ 2^+)$ state, populated in the $^{12}C(p,p')$ reaction at $E_p = 7.7$ MeV. The spectrum in fig. 9a is obtained by summing coincident pulse amplitudes; the system is operated essentially as one single

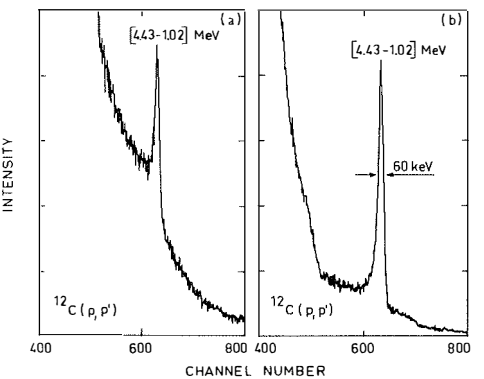

Fig. 9. Pair spectra from the decay of the lowest excited ^{12}C state (4.43 MeV, 2^+), populated in the $^{12}C(p,p')$ reaction at E_p = 7.7 MeV, obtained using a dE/dx + E silicon detector telescope in different modes of operation: (a) total sum spectrum, in which the system is essentially operated as one single detector; (b) coincidence sum spectrum, in which coincident pulses are accepted with an energy window in the dE/dx channel which corresponds to the most probable energy deposited in it by simultaneous transmission of a positron and electron. The high-energy background is strongly reduced. The width of the pair line is determined by the Doppler effect.

detector. The spectrum in fig. 9b shows the performance of the detector telescope. In this case, coincident pulses are accepted with an energy window in the dE/dx channel which corresponds to the most probable energy deposited in it by the simultaneous transmission of a positron and an electron. The disturbing background is substantially reduced. The width of the pair line is due to the Doppler effect.

An obvious limitation of this method is the attainable resolution which is especially worsened by the thin dE/dx detector having a large capacitance. Therefore, this method is suitable only for cases where the width of the pair lines is mainly due to the Doppler effect.

(ii) A NaI(Tl) detector was employed to observe the 511 keV quanta (formed in the annihilation of the positron in the Si(Li) detector) in coincidence with internal pairs[49]. The detector geometry in fig. 10 was used in preliminary tests of this possibility.

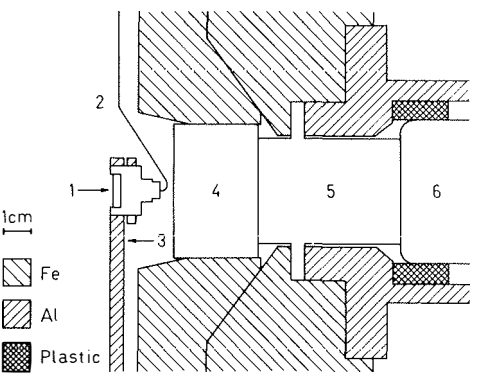

Fig. 10. Detector geometry used in Si(Li)-NaI(Tl) coincidence measurements: (1) Si(Li) detector, (2) to preamplifier, (3) cold finger, (4) NaI(Tl) detector, (5) light guide, (6) PM tube

The high-energy background is reduced typically by a factor of 10 to 15. The coincidence pair-line efficiency for the detector geometry used was 2.3 % of the singles efficiency. Using a better detector geometry and a larger NaI(Tl) detector, it is possible to increase the total absolute efficiency by a factor of up to 10. However, it should be pointed out that the use of a NaI(Tl) coincidence detector does not reduce the high-energy positron background.

A coincidence method combining these two ideas (i) and (ii) was proposed by Michaelis and Lange[30,45], but no actual in-beam applications of this method appear to have been reported, possibly due to the difficulties and limitations discussed above.

The use of a single, thick E detector does not give a reasonable peak-to-background ratio under heavy background conditions. The best background reduction and a fairly high pair-line efficiency are achieved by employing two Si(Li) detectors and a Si(Li)-Si(Li) sum-coincidence tehcnique described in subsect. 3.3.4.

3.3.4. Sum-coincidence technique

In the Si(Li)-Si(Li) sum-coincidence technique[16] two standard Si(Li) detectors and a detector geometry shown in fig. 11 are used. A count is accepted when an electron and a positron enter the opposite counters simultaneously, whereby the pulses from both detectors are summed. The sum-coincidence spectrum is recorded using an energy window in both Si(Li) channels corresponding to the momentum window

of the magnetic lens. The tantalum plate between the detectors removes the counts due to electrons and positrons scattered from one detector to the other.

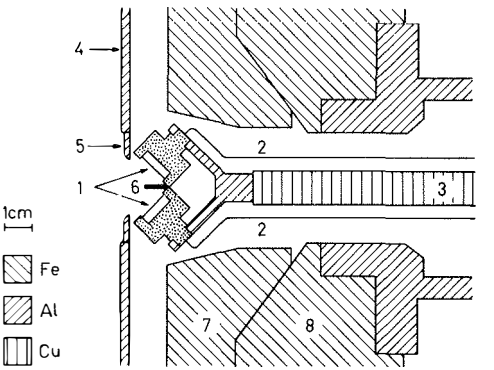

Fig. 11. The detector geometry used in Si(Li)-Si(Li) coincidence measurements: (1) Si(Li) detectors, (2) to preamplifiers, (3) cold finger, (4) cold trap, (5) entrance baffle, (6) Ta plate, (7) extra iron piece, (8) door of the lens spectrometer

The overall efficiency for each detector in the geometry of fig. 11 (for monoenergetic electrons) is about 33 % of the overall efficiency of a single detector in the normal geometry having axial symmetry. The fairly high overall efficiency is understood if one considers the average angles of incidence (with respect to the detector surface plane) in the normal geometry ($\approx 40^{o}$) and in the coincidence geometry ($\approx 90^{o}$), and the corresponding average PTR values, ≈ 0.60 and ≈ 0.85, respectively[2,37].

The performance of the sum-coincidence method is demonstrated in fig. 12, which shows pair spectra from the decay of the ^{64}Zn(1911 keV, 0_2^+) state, populated in the ^{64}Zn(p,p') reaction at E_p = 8.55 MeV. An experimental coincidence pair-line efficiency of 2.1×10^{-4} and a sum-peak energy resolution of 6.4 keV for the 1911 keV E0 pair line are achieved.

The background conditions in recording the 1911 keV pair line are much worse than in the case of the fairly intense 1762 keV E0 transition in ^{90}Zr, demonstrated in subsect. 3.3.2. As the Q value for the ^{64}Zn(p,n) reaction[51] is -7.85 MeV, a β^+-decaying activity ($T_{1/2}$ = 2.6 min) is produced, which gives rise to the main part of the detector counting rates and the high-energy background. The coincidence conditions reduce the high-energy background (mainly caused by the β^+ activity) by a factor of about 200 as compared to the direct spectrum of a single detector. The remaining background is mainly due to random coincidences; therefore, the maximum counting rates of the silicon detectors in the present measurements were kept below 3×10^3 cps.

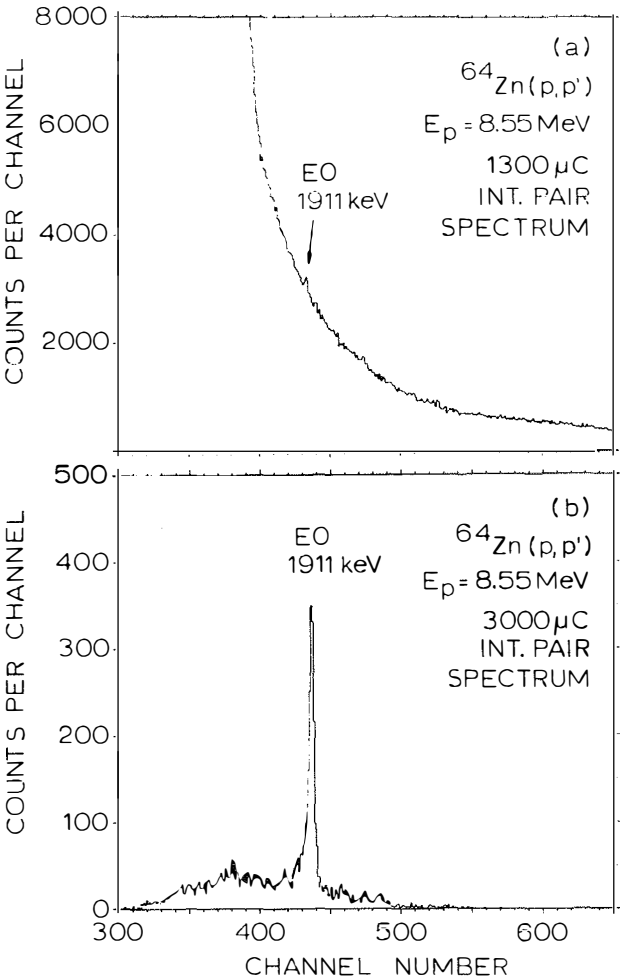

Fig. 12. Internal pair spectra from the decay of the ^{64}Zn(1911 keV, 0_2^+) state, obtained using the detector geometry shown in fig. 11: (a) direct spectrum of a single detector, (b) sum-coincidence spectrum. The target thickness was 0.7 mg/cm^2 and the sum-peak resolution 6.4 keV.

Improved resolution is achieved by employing the digital summing principle. The multiparameter data-acquisition program MUL was used for recording the two-energy spectra (det 1; det 2) and the two time spectra (det 1 - det 2; det 1 - RF) on magnetic tape for subsequent off-line analysis. The block diagram shown in fig. 13 is used for recording the sum-coincidence spectra.

The program EVESUM first sorts the events into a summing matrix, according to given preselection gates: (i) an energy gate in both Si(Li) channels corresponding to the momentum window of the magnetic lens, (ii) a coincidence time gate and (iii) a time gate to select prompt or delayed events. By editing the summing matrix, the user can sum the preselected energy-address pairs multiplied by given constants.

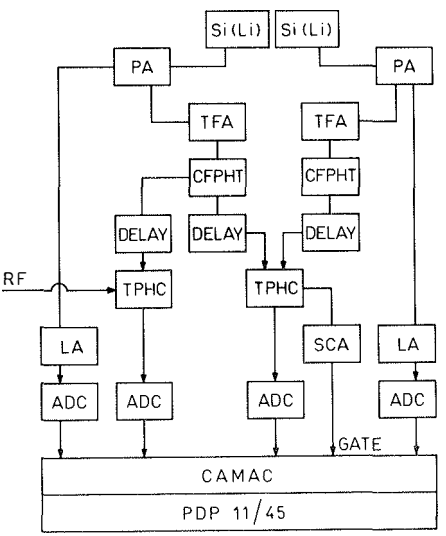

Fig. 13. Schematic block diagram used for recording the sum-coincidence spectra

The improved resolution is demonstrated in fig. 14, which shows pair spectra from the decay of the ^{54}Fe(2561 keV, 0_2^+) state, populated in the ^{54}Fe(p,p') reaction at E_p = 6.9 MeV. A sum-peak energy resolution of 4.8 keV is achieved in agreement with the squared sum of the measured resolutions (3.4 keV) of each detector for 975 keV electrons from ^{207}Bi.

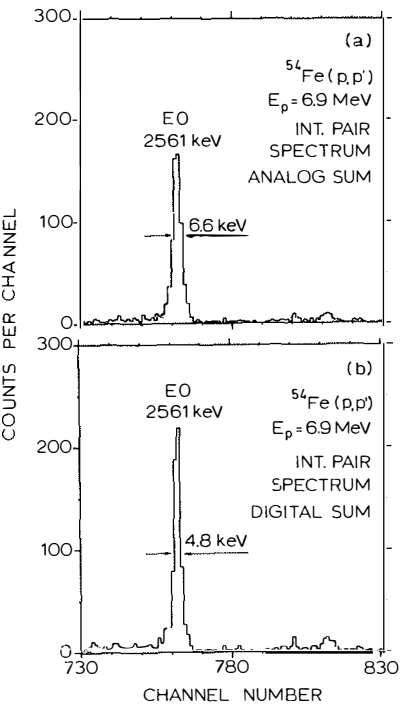

Fig. 14. Internal-pair spectra from the decay of the ^{54}Fe(2561 keV, 0_2^+) state, obtained simultaneously using (a) an analog, (b) a digital summing technique. The target thickness was 0.7 mg/cm^2 and the integrated current 6000 μC.

As shown in subsect. 3.3.2, a single detector can be used in cases where the background level is not too high. The experiments described above demonstrate that an internal-pair-formation spectrometer based on the sum-coincidence technique is a powerful tool for high-resolution in-beam studies of internal-pair transitions under heavy background conditions, e.g. when the (p,n) reaction channel is open.

For the final detector setup, two separate, semicircular Si(Li) detectors* have been ordered to be used instead of the detector geometry of fig. 11. The pair-line efficiency and the sum-peak energy resolution for this detector system are estimated to be $\approx 1.5\times10^{-3}$ and $\lesssim$ 4.0 keV, respectively.

In the pair-line measurements of sect. 4.2 both singles and sum-coincidence detector geometries were used as mentioned therein.

---

* The semicircular detectors are made by Société d'Etude Physique, 11 Rue du Moulin à vent, 91590 Cerny, France.

3.3.5. Pair-line efficiency calculations

In the intermediate-image pair spectrometer, positron-electron pairs are focused from the target onto Si(Li) detector(s) under the following conditions:

(i) both pair components enter the acceptance solid angle, and

(ii) they fall within the momentum band width accepted by the magnetic lens.

The spectrometer pair-line efficiency $\varepsilon_{\ell}^{\pi}(k)$ is defined as the ratio of the observed pair counting rate to the total emission rate of pairs associated with the same transition.

The geometry used in the efficiency calculations is shown in fig. 15, and the angular correlation functions $F_{\ell}(\Theta,\delta,\theta_q,\phi_q,W_+)$ were presented in sect. 2.3. In the pair-line efficiency calculations the azimuthal angle ϕ was used instead of the separation angle Θ ($\cos^2\frac{1}{2}\Theta = 1 - \sin^2\alpha \sin^2\frac{1}{2}\phi$). For the intermediate-image magnetic spectrometer, $\delta = \frac{1}{2}\pi$, and the beam axis is an axis of rotational symmetry, so that F_{ℓ} is independent of ϕ_q. Also, the energies and the momenta of electrons and positrons focused from target to detector(s) are equal, i.e. $W_+ = W_- = \frac{1}{2}k$ and $p_+ = p_- = (\frac{1}{4}k^2 - 1)^{1/2}$.

The ratio of the number of pairs emitted per second into solid angles $d\Omega_+ d\Omega_-$, with the azimuthal angle ϕ between $\bar{p}_+$ and $\bar{p}_-$ and with the positron energy between W_+ and $W_+ + dW_+$, to the total number of pairs emitted per second is

$$F_{\ell}(\phi,\tfrac{1}{2}\pi,\tfrac{1}{2}k)\,d\Omega_+ d\Omega_- dW_+ \times \begin{cases} 1 & \text{for } E0, \\ \left[\Gamma_{\ell}^{\pi}(k)\right]^{-1} & \text{for } \ell \geq 1, \end{cases}$$

where $\Gamma_{\ell}^{\pi}(k)$ is the conversion coefficient for internal pair formation[24,52,53]. The relationship $dW = \frac{p}{W} dp$ is used to convert from momentum to energy units.

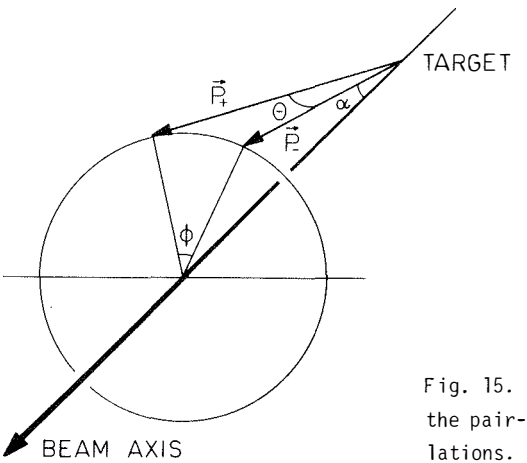

Fig. 15. The geometry used in the pair-line efficiency calculations. The average angle of acceptance of the spectrometer is $\alpha \approx 50^{o}$.

The effects of a finite angular opening are ignored and it is assumed that there is no preferred direction in space, i.e. the m_i substates of the emitting level are equally populated. In the present work, we are concerned mainly with transitions from 0^+ states. These transitions are isotropic and the results of Rose[24] and Oppenheimer[28] for unorientated nuclei are strictly applicable. The validity of different approximations is discussed in more detail at the end of this subsection.

The pair-line efficiency $\varepsilon_{\ell}^{\pi}(k)$ is given by the expression

$$\varepsilon_{\ell}^{\pi}(k) = 8\pi d(k) \left[t f_d \varepsilon_d(k) \right]^2 R_{\pi} (\tfrac{1}{4} k^2 - 1)(4\pi^2 k)^{-1}$$

$$\times \left[\int_0^{2\pi} \gamma_{\ell}(\phi, \tfrac{1}{2} k) d\phi \right] \cdot \begin{cases} 1 & \text{for E0} \\ \left[\Gamma_{\ell}^{\pi}(k) \right]^{-1} & \text{for } \ell \geq 1 \end{cases}$$

$$= 8\pi d(k) \left[\varepsilon_e(k) \right]^2 R_{\pi} \varepsilon'_{\ell}(k) \cdot \begin{cases} 1 & \text{for E0} \\ \left[\Gamma_{\ell}^{\pi}(k) \right]^{-1} & \text{for } \ell > 1, \end{cases}$$

where $d(k)$ is the experimentally determined coincidence efficiency factor, $\varepsilon_e(k) = t f_d \varepsilon_d(k)$ is the spectrometer overall efficiency for monoenergetic electrons, and $R_{\pi} = (\Delta p/p)_{\pi}$ is the observed momentum resolution for pair lines. The factor $d(k)\left[t f_d \varepsilon_d(k) \right]^2 R_{\pi}$ is determined experimentally. The differential internal-pair-formation coefficients γ_{ℓ} for the condition $W_+ = W_-$ are given in appendix III.

In the present work the efficiency factors $\varepsilon'_{\ell}(k)$ for E0, E1, E2 and M1 transitions have been computed for transition energies $2.5 \leq k \leq 16$ employing the formulation of refs. 27, 54 and 55. The results for transition energies up to $k = 12$ are shown in fig. 16 for $\alpha = 50^{\circ}$. The results are consistent with previous calculations by Bent et al.[56] for $\alpha = 41^{\circ}$ and Wilkinson et al.[54] for $\alpha = 45.7^{\circ}$.

The efficiency calculations were carried out for the case of nonaligned nuclei. The transitions from aligned nuclei proceed mainly by emitting gamma rays. Bartholomew et al.[37] point out in their review article that the era of pair spectrometers for gamma-ray measurements is largely past. For most practical applications these instruments have been superseded by Ge(Li) detectors. So the

efficiency calculations presented above are valid for the main area of usefulness still remaining, i.e. for the study of excited 0^+ states and especially their electric monopole decay rate.

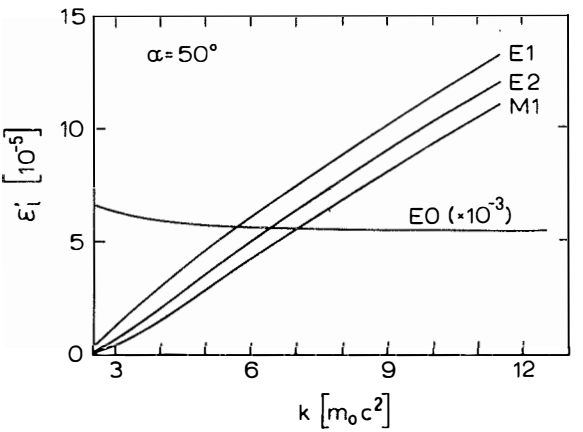

Fig. 16. Calculated efficiency factors $\varepsilon'_\ell(k)$ versus transition energy k for E0, E1, E2 and M1 multipoles.

The zero-order Born approximation, used in the pair-line efficiency calculations, is valid for the condition $Z\alpha/\beta \ll 1$ which has to be fulfilled simultaneously by the velocity $v = \beta c$ of both the electron and the positron; α is the fine-structure constant 1/137. For $Z = 28$ and $k > 1$ the value of $Z\alpha/\beta$ is smaller than 0.27. It should be noted that the Born approximation is most valid for the special condition of the magnetic plus Si(Li) pair spectrometer, i.e. $W_+ = W_- = \frac{k}{2} \geq 1$. Even the energy spectra

of the pair components are almost flat at $W_+ \approx W_-$. Exact calculations[18,31] have shown that the total internal-pair formation coefficient deviates from the Born approximation less than 15 % for $Z < 50$ and $k > 3$.

A value of 50^0 was used for the mean acceptance angle α in the efficiency calculations, this angle having been measured experimentally with an accuracy of ± 3. Fig. 17 shows $\varepsilon'_{\ell}(k)$ curves calculated for different α values. The uncertainty of 1^0 in α corresponds to an uncertainty of about 1 % in the pair-line efficiency.

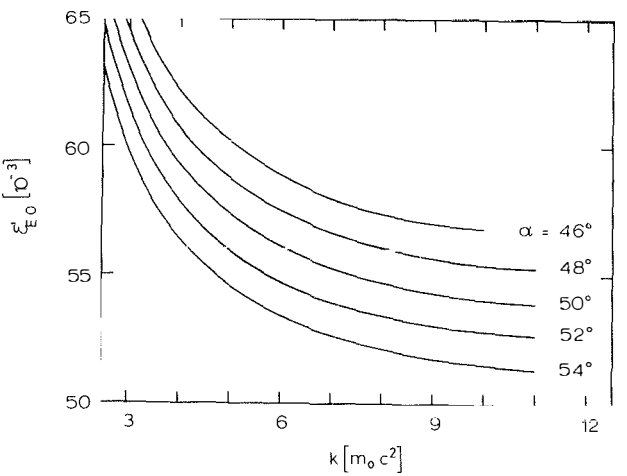

Fig. 17. The pair-line efficiency factor $\varepsilon'_{E0}(k)$ as a function of transition energy for different values of spectrometer mean acceptance angle α

The uncertainty in the calculation of the spectrometer efficiency factors is estimated to be smaller than 6 % for transition energies of k > 3 and for nonaligned nuclei. The uncertainties of the experimentally determined factor $d(k)\,[tf_d\varepsilon_d(k)]^2\,R_\pi$ in the pair-line efficiency function is discussed in detail in subsect. 3.3.6.

3.3.6. In-beam calibration measurements

In order to calibrate the pair spectrometer for further studies of EO internal-pair transitions, we carried out the following measurements, employing mostly the (p,p') reaction at E_p = 6.9 MeV on natural Ca and Zr, and on enriched ^{54}Fe (95.6 %) and ^{64}Zn(98.7 %) targets.

(a) The momentum resolution R_π for pair lines was measured employing the EO($0_2^+ \rightarrow 0_1^+$) transitions in ^{40}Ca (3353 keV) and in ^{90}Zr (1762 keV). The observed value was R_π = 0.15(1) for the detector geometry of fig. 11.

(b) The overall efficiency $\varepsilon_e(k)$ of the spectrometer for monoenergetic electrons in the fixed-current mode was discussed in subsect. 3.2.2. The function $\varepsilon_e(k)$ was measured for all detector geometries separately with the aid of a calibrated ^{207}Bi source.

(c) In the sum-coincidence method there are two types of correction factor: (i) the ratio of the pair-line efficiency in the coincidence mode ε_c to the pair-line efficiency ε_t corresponding to the measurement of the sum of the two Si(Li) detectors in the singles mode and (ii) the efficiency ε_{cc} of the coincidence circuit. The latter correction can be determined in an off-line analysis of the magnetic tapes. The sum-coincidence reduction was measured employing a summing amplifier and

the $E0(0_2^+ \rightarrow 0_1^+)$ transitions in ^{40}Ca (3353 keV) and in ^{90}Zr (1762 keV). The observed value for the detector geometry of fig. 11 is $\varepsilon_c/\varepsilon_t$ = 0.580(15).

(d) In order to test the present efficiency-calibration procedure for conversion-electron and internal-pair spectra, the ratios $W_K(E0)/W_\pi(E0)$ were measured for $E0(0_2^+ \rightarrow 0_1^+)$ transitions in ^{90}Zr and ^{64}Zn. The ^{90}Zr spectra were already presented in subsect. 3.3.1 and the pair-line spectrum of ^{64}Zn in subsect. 3.3.3. The present experimental results are compared in table 2 with a previous result[47] and with the theoretical values of $\Omega_K(E0)/\Omega_\pi(E0)$ calculated in sect. 2.2. The agreement between the present experimental ratios $W_K(E0)/W_\pi(E0)$ and the calculated $\Omega_K(E0)/\Omega_\pi(E0)$ values is good. The previous experimental ratio for ^{90}Zr is 10 % smaller than the ratios observed in this work.

Table 2

Comparison of experimental and theoretical values for the ratio of K conversion and internal pair decay probabilities in the $E0(0_2^+ \rightarrow 0_1^+)$ transitions in ^{90}Zr and ^{64}Zn

Nucleus	$E(0_2^+)$ (keV)	Exp.		Theor.
		$W_K(E0)/W_\pi(E0)$		$\Omega_K(E0)/\Omega_\pi(E0)$
		present work	Nessin et al.[a]	present work
^{90}Zr	1762	2.28(32)	2.08(8)	2.36
^{64}Zn	1911	0.46(7)	-	0.47

a) Ref. 47

(e) The branching ratio $I_\pi(EO; 0_i^+ \rightarrow 0_1^+)/I_K(E2; 0_i^+ \rightarrow 2_1^+)$ is usually derived from an EO pair-line measurement with a fixed momentum window centered at $\frac{1}{2}\left[E(0_i^+) - 2m_0c^2\right]$ and from an E2 conversion-electron measurement with a fixed momentum window at the K conversion line of the E2 transition. The two runs are normalized with the aid of integrated proton currents.

As a final test of the present efficiency factors, we re-examined the EO internal-pair and E2 conversion-electron decay branches from the 0_2^+ state at 2.56 MeV in ^{54}Fe and compared them to the previous result reported in ref. 58.

The singles pair-line spectrum from the $^{54}Fe(p,p')$ reaction at E_p = 6.9 MeV in the energy range of 2.4 to 3.5 MeV is shown in fig. 18. The present EO internal-pair and E2 conversion-electron measurements gave the experimental branching ratio $I_\pi(EO; 0_2^+ \rightarrow 0_1^+)/I_K(E2; 0_2^+ \rightarrow 2_1^+)$ = 14.8(18). When combined with the theoretical E2 conversion coefficient[59], this ratio corresponds to an EO internal-pair decay branch of $1.90(30)\times10^{-3}$, in rather good agreement with the previous result of $1.70(25)\times10^{-3}$ reported in ref. 58.

One can conclude that the methods used for measurements of EO internal-pair-decay branches from excited 0^+ states allow a determination of experimental values to an accuracy of 12 to 20 %.

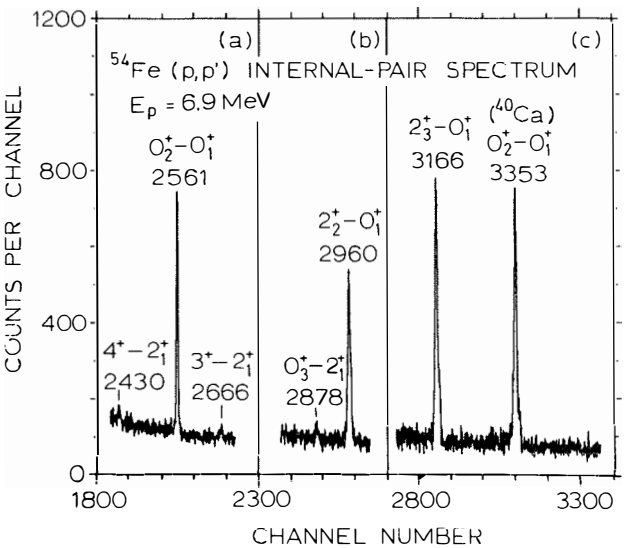

Fig. 18. Pair-line spectrum of ^{54}Fe in the energy range of 2.4 to 3.5 MeV obtained in three separate measurements with fixed momentum windows centered at $\frac{1}{2}\left[E(I_i^\pi) - 2m_0c^2\right]$, where I_i^π is (a) 0_2^+, (b) 2_2^+ and (c) 2_3^+. Target thickness was 0.7 mg/cm^2 and the integrated proton current 6000 μC in each measurement.

4. ELECTROMAGNETIC DECAY OF EXCITED 0^+ STATES IN $^{58,60,62}Ni$

4.1. Introduction

Experimental information on the levels of ^{58}Ni, ^{60}Ni and ^{62}Ni has been obtained from two-particle and alpha-particle transfer reactions, from inelastic scattering of charged particles, neutrons and gamma-rays, as well as from the decay of $^{58,60,62}Cu$ (refs. 32-35). In all even Ni isotopes at least two 0^+ states have been found below 4 MeV. Experimental data on the excited 0^+ states in $^{58,60,62}Ni$ consist to the energy characteristics, gamma-ray decay branches and lifetimes of the 0_2^+ and 0_3^+ states. The EO decay branch has been measured only for the 0_2^+ state in ^{58}Ni (ref. 14). EO decay measurements for higher 0^+ states are completely missing.

The observed properties of low-lying states in the even nickel isotopes have led to a variety of theoretical descriptions (see ref. 12 for the relevant references). Comparisons of experimental and calculated level schemes have been presented by Hsu and French[60] ($^{58,60,62}Ni$) and by Ballini et al.[61] (^{60}Ni), among others.

Detailed shell-model calculations[9-12] with modified and adjusted surface-delta interactions have been made assuming a closed $^{56}_{28}Ni_{28}$ core, with the added neutrons occupying the $2p_{3/2}$, $2p_{1/2}$ and $1f_{5/2}$ orbitals. The calculations have had a good degree of success in describing the general features of the energy level schemes at excitation energies below 3 MeV. However, calculations of electromagnetic transition rates in terms of an effective charge for the neutrons do not reproduce the experimental results, and there is evidence for excitation of the ^{56}Ni core.

The even nickel isotopes also display some characteristics of vibrational nuclei, such as a triplet of two-phonon states of spin and parity 0_2^+, 2_2^+, 4_1^+ at roughly twice the energy of the one-phonon state 2_1^+. However, the two-phonon character of each 0_2^+ state has to be discussed separately on the basis of the experimental results.

The most extensive theoretical work on E0 decay in the f-p shell has been performed for some transitions in the region of the doubly magic nuclei ^{40}Ca and ^{48}Ca (refs. 44, 63). However, there are no calculations for E0 transition rates around the third doubly magic nucleus ^{56}Ni. For shell-model predictions of the monopole matrix elements one would need an extension of the model space[64].

There is an apparent need for additional information on the electromagnetic decay of excited 0^+ states in the Ni isotopes, especially on their E0 conversion processes (pair or electron). The E0 transition probability depends on the behaviour of the wave functions within the nucleus.

In the present work the E0 branching ratios of excited 0^+ states in ^{58,60,62}Ni were determined by employing the intermediate-image plus Si(Li) spectrometer conventionally in conversion-electron measurements and, after removal of the baffles designed to stop positrons, as a pair spectrometer for pair-line measurements. Furthermore, gamma-ray spectra were recorded with Ge(Li) detectors. Ratios of reduced E0 and E2 transition probabilities (X values) were obtained for the 0^+ states in ^{58,60,62}Ni, for the 0_3^+ states in ^{58,60}Ni and for the 0_4^+ state in ^{60}Ni, which was identified for the first time in the present work. The results are combined with the available lifetimes of the 0_2^+ and 0_3^+ states to extract the monopole strengths. The nature of excited 0^+ states is discussed.

4.2. Measurements

4.2.1. General

In all of the experiments reported in this work, ion beams from the Jyväskylä 90 cm cyclotron were used. Isotopic compositions and thicknesses of the metallic, self-supporting nickel targets are given in table 3.

For all isotopes, the following measurements were carried out employing the (p,p') reaction, mostly at E_p = 6.9 MeV:

(a) singles gamma-ray measurements,

(b) anti-Compton gamma-ray measurements,

(c) γp coincidence measurements,

Table 3

Isotopic compositions and thicknesses of the metallic self-supporting nickel targets employed in the present work

Isotope	Target thickness (mg/cm^2)	Isotopic composition (%) ^{58}Ni	^{60}Ni	^{61}Ni	^{62}Ni	^{64}Ni
^{58}Ni	0.8; 1.4	97.5	1.4	-	0.1	1.0
^{60}Ni	0.5; 0.9	0.7	99.1	-	0.2	-
^{62}Ni	0.5; 1.1	1.4	1.2	0.2	97.2	-

(d) singles conversion-electron measurements for transition energies up to 2.4 MeV,

(e) singles and sum-coincidence pair-line measurements for the decay of excited 0^+ states via E0 and E2 transitions in the energy range from 2.0 to 4.0 MeV.

The present work was undertaken in order to identify low-lying 0^+ states in nickel isotopes and to determine their electromagnetic decay branches, especially E0 internal-pair transition rates. The 0^+ assignments of excited states are usually based on observed E0 transitions in the present internal-pair spectra with no corresponding lines in the gamma-ray spectra. For a firm identification of E2 and M1 transitions de-exciting 0^+ states, γp coincidence measurements were occasionally carried out.

4.2.2. Measurements on ^{58}Ni

The electromagnetic decay of the 0_2^+ state in ^{58}Ni at 2.94 MeV has been investigated in several studies[32,33]. The present experimental branching ratios were determined by adopting the value of 83(3) % for the $M1(0_2^+ \rightarrow 1_1^+)$ transition from previous measurements. The branching ratios of the $E2(0_2^+ \rightarrow 2_2^+)$ and $E2(0_2^+ \rightarrow 2_1^+)$ transitions, deduced from the present singles and anti-Compton gamma-ray measurements, are 8(2) % and 9(2) %, respectively. The conversion coefficient[59] $\alpha_{E2}(0_2^+ \rightarrow 2_2^+;\ 166.6\ \text{keV}) \approx 0.08$ has been taken into account. The high-energy part of the anti-Compton gamma-ray spectrum from the $^{58}Ni(p,p')$ reaction at $E_p \approx 6.9$ MeV is shown in fig. 19.

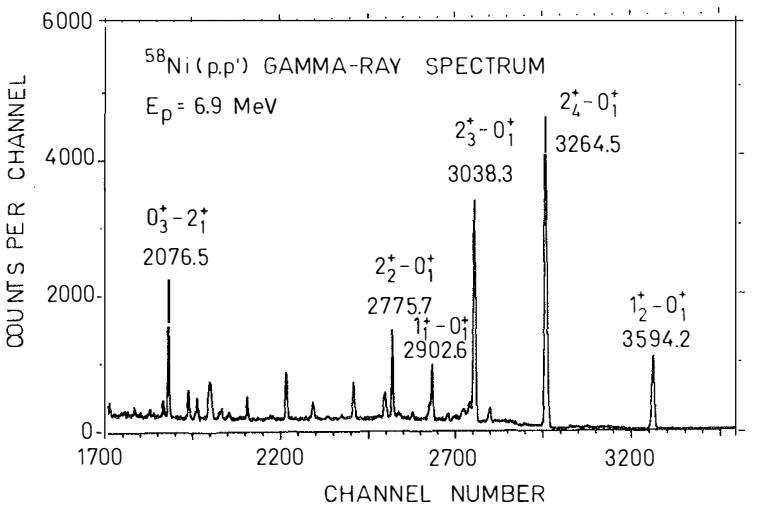

Fig. 19. Partial anti-Compton gamma-ray spectrum from the reaction ^{58}Ni(p,p') at E_p = 6.9 MeV. Only the ground-state transitions and the E2($0_3^+ - 2_1^+$) transition in ^{58}Ni are labelled. The target thickness was 1.4 mg/cm^2.

The E0 internal-pair decay of the 0_2^+ state was studied employing the sum-coincidence technique described in subsect. 3.3.4. Fig. 20 shows a partial pair-line spectrum of the ground-state decay of the excited states in ^{58}Ni in the energy range of 2.6 to 3.1 MeV. The widths of the pair lines are different due to the Doppler effect corresponding to the different lifetimes of the levels[32]. For comparison, a spectrum recorded in a previous work with the Brookhaven

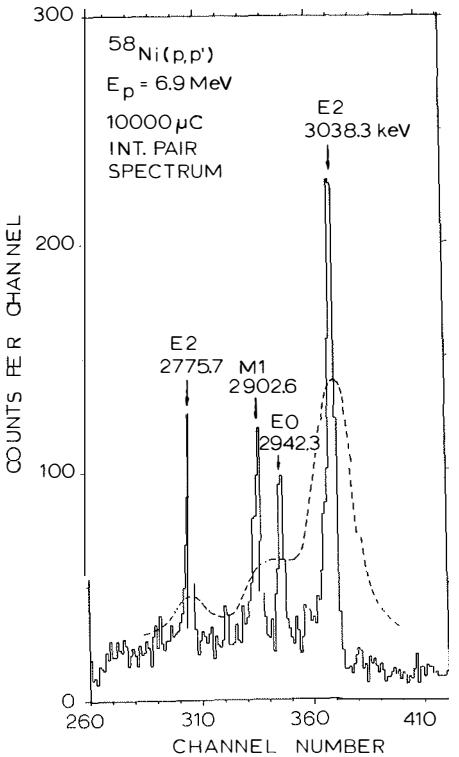

Fig. 20. Partial pair line spectrum of the ground-state transitions from the excited states of ^{58}Ni in the energy range of 2.6 to 3.1 MeV, obtained employing the sum-coincidence technique with a fixed momentum window centered at $\frac{1}{2}[E(0_2^+) - 2m_0c^2]$. The target thickness was 0.8 mg/cm^2. The spectrum recorded in a previous work with the BNL magnetic-lens pair spectrometer[14] is sketched by a dashed curve.

(BNL) magnetic-lens pair spectrometer[14] is sketched in the figure by a dashed curve. The result for the $E0(0_2^+ \rightarrow 0_1^+)$ internal-pair-decay branch of $2.0(4)\times10^{-4}$ is in agreement with the value of $2.2(5)\times10^{-4}$ in ref. 14.

The present internal-pair measurements fix the 0_3^+ state in ^{58}Ni at 3530.9 MeV. The uncertainty in the previous measurements is clearly seen in the latest summary of nuclear level schemes[32] showing a 0_3^+ state at 3.58 MeV. A partial internal-pair spectrum in the energy range of 3.3 to 3.8 MeV is shown in fig. 21. From the γp coincidence measurement it was observed that the 0_3^+ state decays only via an E2 gamma-ray transition to the 2_1^+ state. An upper limit of 3 % was determined for the $0_3^+ \rightarrow 1_1^+$ transition.

Branching ratios for the decay of the 0_3^+ state are derived from singles conversion-electron and sum-coincidence internal-pair spectra. The ratio $I_\pi(E0;\ 0_3^+ \rightarrow 0_1^+)/I_K(E2;\ 0_3^+ \rightarrow 2_1^+) = 13.9(22)$ is deduced from these measurements. When the theoretical E2 conversion coefficient[59] $\alpha_K(E2) = 4.8 \times 10^{-5}$ is taken into account, an E0 internal-pair decay branch of $7.0(11)\times10^{-4}$ is obtained. An independent value for the E0 branch was derived from pair-line measurements of the $E2(0_3^+ - 2_1^+)$ and $E0(0_3^+ \rightarrow 0_1^+)$ transitions. These spectra give a value $I_\pi(E0)/I_\gamma(E2) = 6.7(10)\times10^{-4}$, in good agreement with the former one.

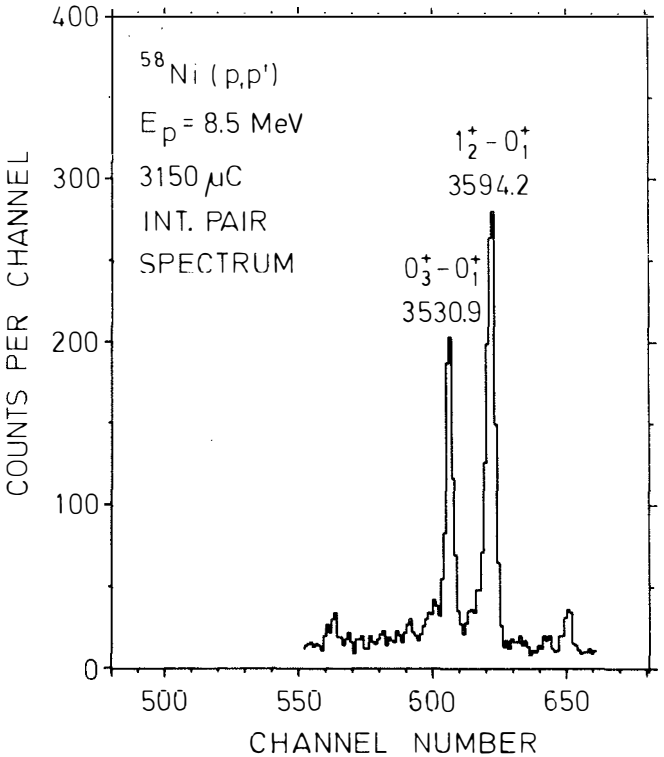

Fig. 21. Partial pair-line spectrum of the ground-state transitions from the excited states of ^{58}Ni in the energy range of 3.3 to 3.8 MeV, obtained using the sum-coincidence technique with a fixed momentum window centered at $\frac{1}{2}[E(0_3^+) - 2m_0c^2]$. The target thickness was 1.4 mg/cm^2.

4.2.3. Measurements on ^{60}Ni

In previous measurements[32,34] the 0_2^+ state in ^{60}Ni at 2.28 MeV is well identified. However, there are some annoying ambiguities about the states at 3.32 MeV and 3.53 MeV. These states are tentatively suggested as 0^+ state on the basis of (^6Li,d) and (^3He,n) studies[65,66]. EO measurements in ^{60}Ni are completely missing.

The EO/E2 branching ratio of the 0_2^+ state was obtained from the singles conversion-electron spectrum shown in fig. 22. The resulting value for the ratio of the K conversion-electron intensities is $I_K(EO;\ 0_2^+ \rightarrow 0_1^+)/I_K(E2;\ 0_2^+ \rightarrow 2_1^+) = 0.074(16)$.

The EO internal-pair decay of the 0_2^+ state was measured in order to determine the experimental value for the ratio of K conversion and internal-pair-formation processes. The observed ratio of 0.130(28), deduced from the pair-line spectrum of fig. 23 and from conversion-electron measurements, is in good agreement with the theoretical value of 0.135 (sect. 2.2).

The anti-Compton gamma-ray spectrum and the pair-line spectrum of transitions in ^{60}Ni in the energy range of 3.2 to 3.6 MeV are shown in fig. 24. The strong internal-pair lines at 3318.3 keV and 3588.0 keV with no corresponding gamma-ray lines confirm the 0^+ assignment of these states.

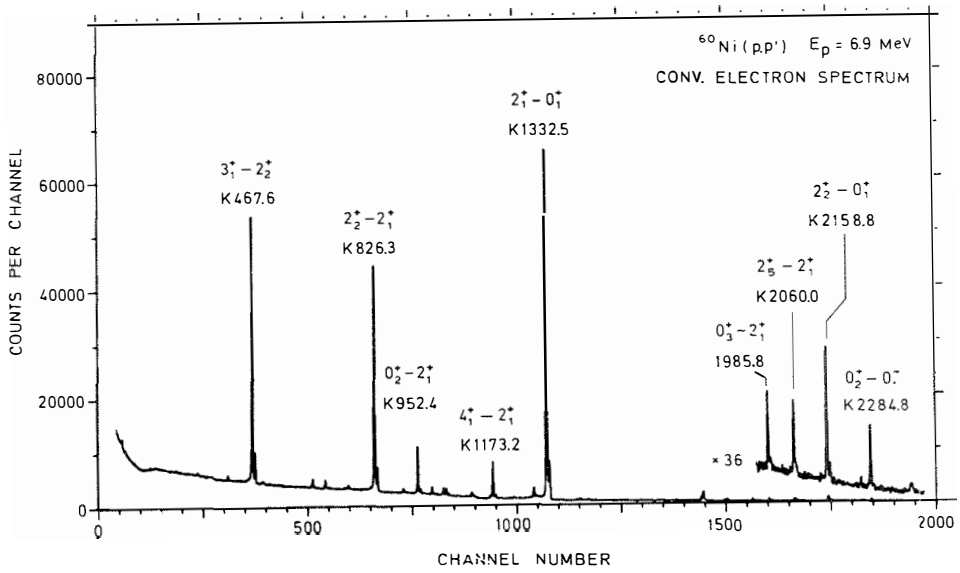

Fig. 22. Singles conversion-electron spectrum from the ^{60}Ni(p,p') reaction at E_p = 6.9 MeV. Only some strong transitions in ^{60}Ni are labelled. The target thickness was 0.9 mg/cm^2.

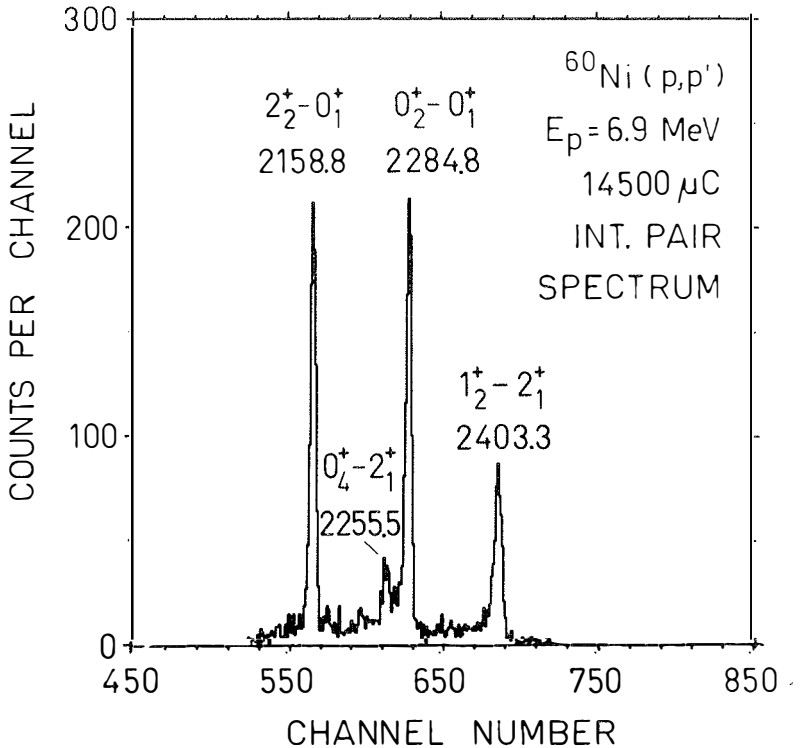

Fig. 23. Partial internal-pair spectrum of ^{60}Ni in the energy range of 2.1 to 2.5 MeV obtained using the sum-coincidence technique with a fixed momentum window at $\frac{1}{2}[E(0_2^+) - 2m_0c^2]$. The target thickness was 0.9 mg/cm^2.

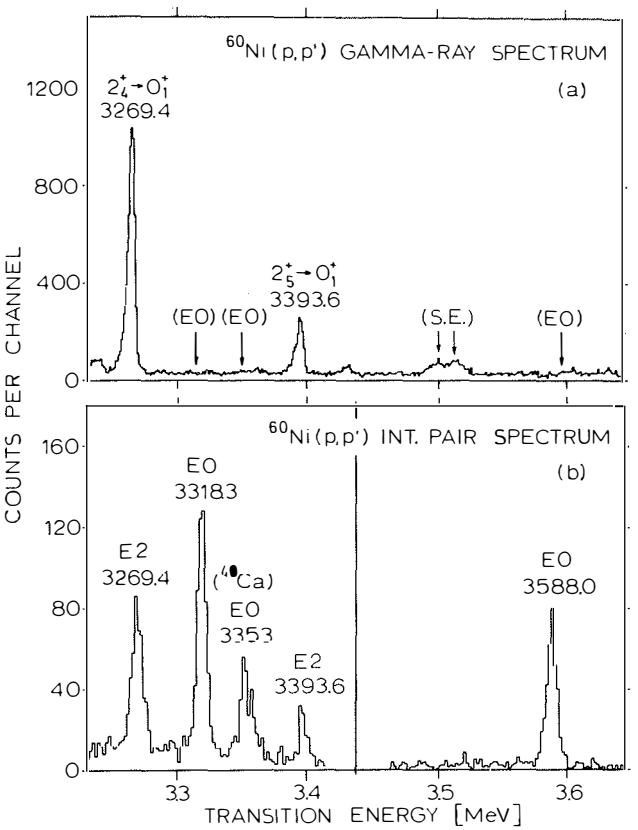

Fig. 24. Spectra of the ground-state transitions from the excited states of ^{60}Ni in the energy range of 3.2 to 3.6 MeV: (a) anti-Compton gamma-ray spectrum (the positions of EO transitions are shown by arrows), (b) pair-line spectrum obtained using sum-coincidence technique in two separate measurements with fixed momentum windows centered at $\frac{1}{2}\left[E(0^+_{3,4}) - 2m_0c^2\right]$. The target thickness was 0.9 mg/cm^2 and E_p = 6.9 MeV.

The γp coincidence measurements were carried out in order to identify the E2 and M1 transitions de-exciting the 0_3^+ and 0_4^+ states. Only the E2($0_3^+ - 2_1^+$) gamma-ray transition was observed to de-excite the 0_3^+ state. Fig. 25 shows a gamma-ray spectrum in coincidende with protons populating the 0_4^+ state. The E2($0_4^+ \rightarrow 2_1^+$), E2($0_1^+ \rightarrow 2_2^+$) and M1($0_1^+ \rightarrow 1_1^+$) transitions are observed. The branching ratios for these transitions were deduced from the anti-Compton gamma-ray measurement: 26(3) %, 57(5) % and 17(3) %, respectively. From a search for the $0_2^+ \rightarrow 2_2^+$ or $0_3^+ \rightarrow 1_1^+$ transitions in γp coincidence and anti-Compton gamma-ray spectra, an upper limit of 3 % for each transition was obtained.

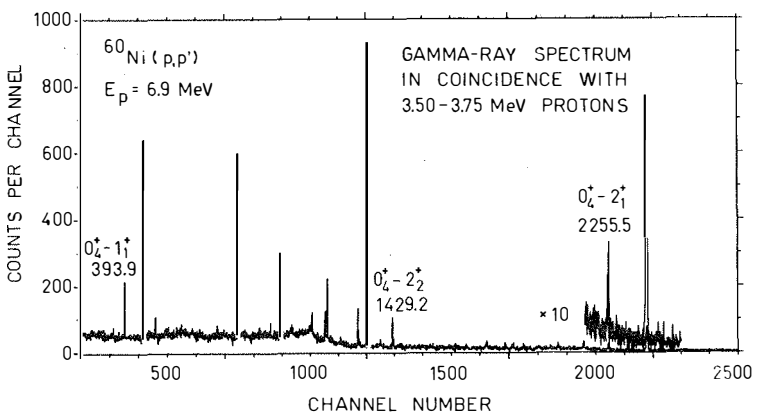

Fig. 25. The gamma-ray spectrum measured in coincidence with 3.50-3.75 MeV protons from the ^{60}Ni(p,p') reaction. Only the gamma-ray transitions de-exciting the 0_4^+(3588.0 keV) state in ^{60}Ni are indicated.

From anti-Compton gamma-ray, singles conversion-electron and sum-coincidence pair-line spectra, the following branching ratios are derived:

$$I_\pi(E0;\ 0_3^+ \to 0_1^+)/I_K(E2;\ 0_3^+ \to 2_1^+) = 11.5(12),$$
$$I_\pi(E0;\ 0_4^+ \to 0_1^+)/I_K(E2;\ 0_4^+ \to 2_1^+) = 68(11).$$

When combined with theoretical E2 conversion coefficients[59], these results correspond to E0 internal-pair-decay branches of $6.2(10)\times10^{-4}$ and $7.4(12)\times10^{-4}$ for the 0_3^+ and 0_4^+ states, respectively.

There exists only a lower limit of 1.5 ps for the half-life of the ^{60}Ni(0_2^+) state obtained employing the Doppler-shift attenuation method[32]. There are no measurements of the lifetime of the ^{60}Ni(0_4^+) state. In the present work, a walk-free centroid method[3], based on the proton-gamma coincidence measurement and the use of a pulsed beam, was used to determine an upper limit of 40 ps for the half-lives of the 0_2^+ and 0_4^+ states in ^{60}Ni.

4.2.4. Measurements on ^{62}Ni

In ^{62}Ni the excited states at 2.05 and 2.89 MeV are assigned spin-parity 0^+ on the basis of (p,t) and (t,p) studies[67,68]. A 0_4^+ assignment is suggested[65] for the 3.52 MeV state excited in the (^{6}Li,d) reaction with the same cross section as the 0_3^+ states in ^{58}Ni and ^{60}Ni. No previous E0 measurements exist for ^{62}Ni.

The gamma decay of excited 0^+ states was studied by γp coincidence measurements. Fig. 26 shows the decay of the 0_2^+ and 0_3^+ states; only the cascade via the 2_1^+ state is observed.

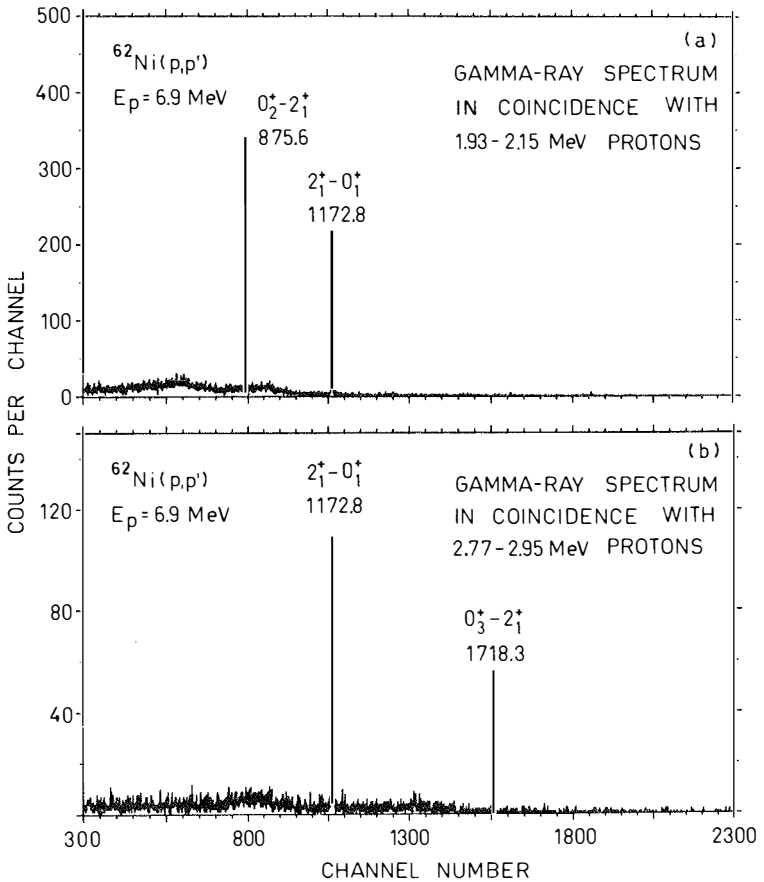

Fig. 26. Coincidence gamma-ray spectra illustrating the decay of (a) the 0_2^+(2048.4 keV) and (b) the 0_3^+(2891.1 keV) states of ^{62}Ni. The gamma-ray spectra measured in coincidence with 1.93-2.15 MeV and 2.77-2.95 MeV protons from the ^{62}Ni(p,p') reaction (E_{p_2} = 6.9 MeV) are shown. The target thickness was 1.1 mg/cm^2.

The X(E0/E2) value for the 0_2^+ state was obtained as an average of singles conversion-electron measurements at proton energies of 4.9 and 6.9 MeV. Fig. 27 shows the high-energy part of the latter measurement. The observed branching ratio expressed as a ratio of K conversion-electron intensities is $I_K(E0; 0_2^+ \rightarrow 0_1^+)/I_K(E2; 0_2^+ \rightarrow 2_1^+)$ = 0.102(14).

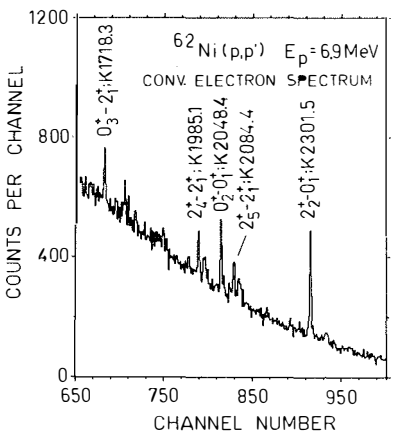

Fig. 27. Singles conversion-electron spectrum from the ^{62}Ni(p,p') reaction at E_p = 6.9 MeV. Only the transitions in the energy range of 1.65-2.50 MeV are shown. The target thickness was 1.1 mg/cm^2.

For ^{62}Ni, the threshold of the ^{62}Ni(p,n) reaction[51] is -4.73 MeV. Rapid accumulation of positron-emitting ^{62}Cu ($T_{1/2}$ = 9.76 min) in the target is unavoidable. The main counting rate of each Si(Li) detector is caused by this activity. As pointed out in subsect. 3.3.3, high counting rates of Si(Li) detectors result in random coincidences and thus disturbing background counts to the pair-line spectra. It is evident that pair-line measurements in ^{62}Ni are possible only with a very low ion beam and a high pair-line efficiency. Measurement of the $E0(0_3^+ \rightarrow 0_1^+)$ and $E0(0_4^+ \rightarrow 0_1^+)$ internal-pair branches remains to be made, employing the semicircular-detector geometry mentioned in subsect. 3.3.4.

4.3. Results

The total E0, M1 and E2 decay branching ratios from excited 0^+ states in $^{58,60,62}Ni$ as determined in this work are presented in fig. 28. Some states of similar decay characteristics are connected by dashed lines as discussed in more detail in sect. 4.4.

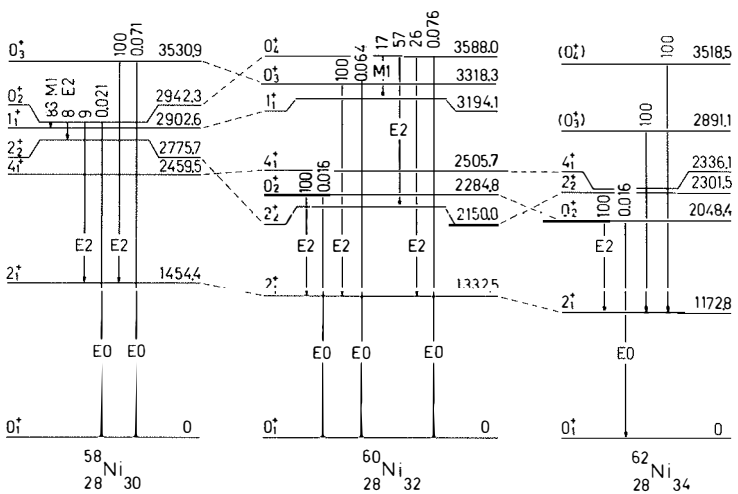

Fig. 28. Electromagnetic decay of 0^+ states in $^{58,60,62}Ni$. Total branching ratios determined in this work are shown. Dashed lines connect some states of similar decay characteristics. The proposed (refs. 32, 65) 0_3^+ and 0_4^+ states in ^{62}Ni are included.

The present experimental results for the 2942.3 keV state in ^{58}Ni, the 2284.8 keV state in ^{60}Ni and the 2048.4 keV state in ^{62}Ni are consistent with the earlier $I^{\pi} = 0_2^+$ assignments. The internal-pair measurements confirm the $I^{\pi} = 0_3^+$ assignment of the 3530.9 keV state in ^{58}Ni and the 3318.3 keV state in ^{60}Ni, and yield a spin and parity assignment of $I^{\pi} = 0_4^+$ for the 3588.0 keV state in ^{60}Ni.

The experimental ratios of the reduced E0 and E2 transition probabilities X(E0/E2) are presented in table 4. The results are combined with the available lifetimes[32] of excited 0_2^+ and 0_3^+ states to extract the monopole strengths $\rho^2(0_i^+ \rightarrow 0_1^+)$. The B(M1), B(E2) and ρ^2(E0) values are included in table 4.

The E0 matrix element M(E0) depends on the monopole strength parameter ρ(E0) by the relation

$$|M(E0)| = |\rho(E0)| \cdot R_0^2 ,$$

where R_0 is the nuclear radius (1.20 $A^{1/3}$ fm). Wilkinson[19] has proposed a single-particle estimate for E0 matrix elements in internal-pair decay as

$$|M_{\pi}^{sp}| = 0.65\ A^{2/3}\ fm^2.$$

In the shell-model sense, the nuclei ^{40}Ca, ^{48}Ca and ^{56}Ni in the f-p shell are doubly magic. Table 5 presents a comparison of the available experimental values for the E0 strengths $|\rho/\rho^{sp}|^2$ expressed in terms of the Wilkinson unit and for the E0 matrix element $|M_{\pi}(E0)|$ in the region of these doubly magic nuclei. The E0 internal-pair

Table 4.

Electromagnetic decay of 0^+ states in $^{58,60,62}Ni$

		^{58}Ni		^{60}Ni		^{62}Ni
$T_{1/2}(0_2^+)$	[ps]	a) $2.01(7)\cdot10^3$	b)	<40 >1.5	c)	$0.76(^{+76}_{-28})$
$B(M1;\ 0_2^+-1_1^+)$	[W.u.]	0.086(8)		-		-
$B(E2;\ 0_2^+-2_2^+)$	[W.u.]	12(2)		-		-
$B(E2;\ 0_2^+-2_1^+)$	[W.u.]	$2.6(5)\cdot10^{-4}$		>1.3 <36		100(55)
$X(E0/E2;\ 0_2^+-2_2^+)$		$1.7(3)\cdot10^{-5}$		-		-
$X(E0/E2;\ 0_2^+-2_1^+)$		d) 0.84(18)	e)	0.027(4)		0.034(5)
$10^3\cdot\rho^2(0_2^+-0_1^+)$		d) 0.0062(12)		>1 <28		100(55)
$T_{1/2}(0_3^+)$	[ps]	a) 0.19(6)		$0.24(^{+28}_{-12})$		>3.1
$B(E2;\ 0_3^+-2_1^+)$	[W.u.]	5.6(16)		$5.5(^{+50}_{-30})$		<0.84
$X(E0/E2;\ 0_3^+-2_1^+)$		0.47(8)		0.49(8)		
$10^3\cdot\rho^2(0_3^+-0_1^+)$		80(32)		77(42)		
$T_{1/2}(0_4^+)$	[ps]			<40	b)	
$B(M1;\ 0_4^+-1_1^+)$	[W.u.]			$>1.5\cdot10^{-3}$		
$B(E2;\ 0_4^+-2_2^+)$	[W.u.]			>1.4		
$B(E2;\ 0_4^+-2_1^+)$	[W.u.]			$>4.5\cdot10^{-3}$		
$X(E0/E2;\ 0_4^+-2_2^+)$				0.13(3)		
$X(E0/E2;\ 0_4^+-2_1^+)$				2.9(5)		
$10^3\cdot\rho^2(0_4^+-0_1^+)$				>0.37		

a) From ref. 32.

b) Uncertainty of the last figures is given in parentheses.

c) Upper limit obtained in this work employing the method described in ref. 3.

d) The spherical-vibrator values for nickel isotopes[69,70] are $X_{vibr} = \beta^2_{rms} \approx 0.039$ and $\rho^2_{vibr} = (0.151\cdot Z\beta^2_{rms})^2 \approx 27\cdot10^{-3}$.

e) Previous value obtained in ref. 14: $X(E0/E2) = 0.97 \pm 0.24$.

f) $B(M1)_{W.u.} = 1.79\ \mu_N^2$

g) $B(E2)_{W.u.} = 5.94\times10^{-6}\ A^{4/3}\ e^2b^2$.

Table 5.

Summary of data on excited 0^+ states of nuclei in the Ca-Ni region

Nucleus	$E(0_i^+)$ (keV)		τ [a] (ps)	$\Gamma_\pi(E0)/\Gamma$	$\lvert M_\pi \rvert$ (fm^2)	E0 strength [b] $\lvert \rho/\rho^{sp} \rvert^2$	Ref.
$^{38}_{18}Ar_{20}$	0_2^+	3380	29(3)	$6.6(10)\times10^{-3}$	2.26	0.095(18)	c)
$^{40}_{20}Ca_{20}$	0_2^+	3353	$3.17(22)\times10^{3}$	1.0	2.6	0.12(1)	d)
	0_3^+	5212	1.9(3)	$<1.4\times10^{-3}$	<1.0	<0.02	"
$^{42}_{20}Ca_{22}$	0_2^+	1836	480(30)	$2.05(17)\times10^{-2}$	5.93	0.56(9)	"
$^{44}_{20}Ca_{24}$	0_2^+	1883	20(6)	$8.8(14)\times10^{-4}$	5.4	0.43(28)	"
$^{48}_{20}Ca_{28}$	0_2^+	4284	322(16)	0.225(8)	1.52	0.036(4)	"
$^{54}_{26}Fe_{28}$	0_2^+	2561	$\geq$2.0	$1.9(3)\times10^{-3}$	$\leq$9.8	$\leq$1.14	present work
	0_3^+	4289	$0.080(^{+24}_{-20})$	$<5.8\times10^{-4}$	<6.1	<0.44	"
$^{58}_{28}Ni_{30}$	0_2^+	2942	2.9(1)	$2.0(4)\times10^{-4}$	0.054	$3.1(7)\times10^{-5}$	"
	0_3^+	3531	0.28(8)	$7.0(11)\times10^{-4}$	6.08	0.39(16)	"
$^{60}_{28}Ni_{32}$	0_2^+	2284	<58 >2.2	$1.4(2)\times10^{-4}$	>0.70 <3.68	$>4.9\times10^{-3}$ <0.14	"
	0_3^+	3318	$0.35(^{+41}_{-16})$	$6.2(10)\times10^{-4}$	6.11	0.38(20)	"
	0_4^+	3588	<58	$7.4(12)\times10^{-4}$	>0.42	$>1.8\times10^{-3}$	"
$^{62}_{34}Ni_{34}$	0_2^+	2048	$1.1(^{+11}_{-4})$	$1.25(20)\times10^{-4}$	7.11	0.49(26)	"

a) From ref. 32.

b) See ref. 19.

c) From ref. 71.

d) From ref. 44.

branches are also included in table 5. The strengths of the $E0(0^+_{2,3} \rightarrow 0^+_1)$ transitions in s.p.u. are plotted as a function of mass number in fig. 29.

The E0 transitions from the excited 0^+ states to the ground state are usually in competition with an E2 gamma cascade via an $I^\pi = 2^+$ intermediate state. The latter then represents almost the total width of the excited 0^+ state. As seen from table 5, the ratio $\Gamma_\pi(E0)/\Gamma(E2)$ is of the order of 10^{-3}, with some exceptions (e.g. ^{48}Ca).

In fig. 29, a systematic behaviour of the strength across the shell is observed; the greatest strengths occur in the middle of the shells.

Large monopole strengths measured for the $E0(0^+_2 \rightarrow 0^+_1)$ transitions in $^{42,44}Ca$ are explained[44,63] by assuming significant proton-particle-hole components in the wave functions of both ground and excited 0^+ states. In contrast, ^{48}Ca appears to be a good closed-shell nucleus, and the monopole strength in this isotope is indeed very small (0.036). This value is of the same order of magnitude as the recent result[8] of $|\rho/\rho^{sp}|^2 = 0.060(7)$ for the $E0(0^+_2 \rightarrow 0^+_1)$ transition in the doubly magic $^{146}_{64}Gd_{82}$.

The excitation energy of the 0^+_2 state for the even nickel isotopes strongly decreases when going away from the doubly magic ^{56}Ni and goes through a minimum at mass number 62. At the same time the monopole transition strength from the 0^+_2 state to the 0^+_1 ground state increases strikingly when going from ^{58}Ni to ^{62}Ni.

The large monopole strengths (of the same order as in $^{42,44}Ca$) measured for the $E0(0^+_2 \rightarrow 0^+_1)$ transition in ^{62}Ni and for the $E0(0^+_3 \rightarrow 0^+_1)$ transitions in ^{60}Ni indicate significant core-excited components.

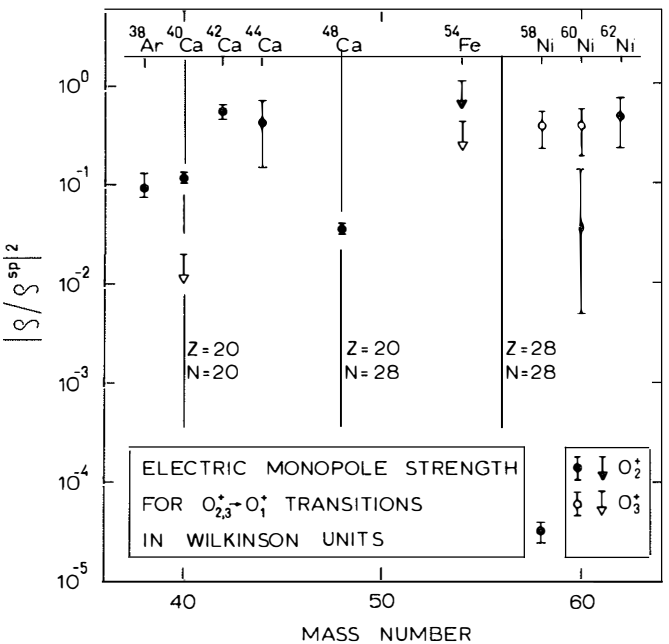

Fig. 29. E0 single-particle strengths (see ref. 19) in the region of doubly magic nuclei $^{40}_{20}Ca_{20}$, $^{48}_{20}Ca_{28}$ and $^{56}_{28}Ni_{28}$ as a function of mass number for the $E0(0^+_{2,3} \rightarrow 0^+_1)$ internal-pair decay. The strength of the $E0(0^+_2 \rightarrow 0^+_1)$ transition in ^{60}Ni is obtained by assuming that the speed of the competing E2 transition is 10 W.u. (the experimental lower and upper limits are also shown).

4.4. Discussion

The experimental level schemes of even nickel isotopes have the familiar pattern of a vibrational nucleus with a low-lying 2_1^+ state and a triplet of 0_2^+, 2_2^+ and 4_1^+ states at about twice the energy of the 2_1^+ state as shown in fig. 30. The splittings in the 0_2^+, 2_2^+, 4_1^+ triplet change from one isotope to the next. The changes are quite well accounted for by the detailed shell-model calculations[9-12], as shown in table 6.

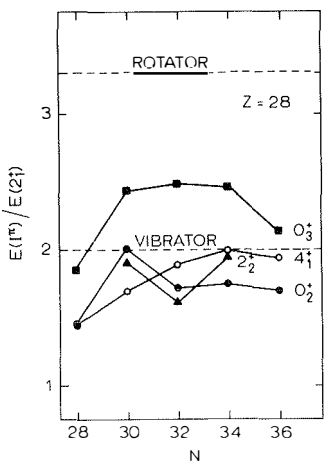

Fig. 30. The experimental energy ratio $E(I^\pi)/E(2_1^+)$ for some low-lying levels in even nickel isotopes according to refs. 32-35 and the present results

Table 6

Comparison of some experimental and calculated level energies of $^{58,60,62}Ni$. The experimental values are based on refs. 32-35 and on the present results and are compared with shell-model calculations of Auerbach[10], Cohen et al.[9] and Glaudemans et al.[11].

Nuclear level	I	Level energies (MeV) exp.	Auerbach	Cohen et al.	Glaudemans et al.
^{58}Ni	0_3^+	3.53 a)	3.75	4.23	4.25
	0_2^+	2.94	2.72	2.54	3.04
	4_1^+	2.46	2.46	2.29	2.38
	2_2^+	2.77	2.92	2.88	2.67
	2_1^+	1.45	1.44	1.31	1.50
^{60}Ni	0_4^+	3.59 a)	3.55	-	-
	0_3^+	3.32 a)	2.98	3.27	-
	0_2^+	2.28	2.27	2.32	2.48
	4_1^+	2.51	2.50	2.20	2.34
	2_2^+	2.16	2.36	2.17	2.19
	2_1^+	1.33	1.55	1.42	1.55
^{62}Ni	(0_3^+)	2.89	2.34	2.61	-
	0_2^+	2.05	2.08	2.01	2.09
	4_1^+	2.34	2.60	2.20	2.43
	2_2^+	2.30	2.40	2.25	2.28
	2_1^+	1.17	1.56	1.53	1.45

a) From the present work.

Better agreement has been achieved in the description of ^{60}Ni than of ^{58}Ni (e.g. excited 0^+ states in ^{58}Ni are too widely separated). One would assume that the added neutrons in ^{60}Ni as compared to ^{58}Ni would act to diminish the effect of neutron core excitation. On the other hand, the calculations[62] have indicated that proton core-excited states may contribute significantly to nickel isotopes beyond ^{60}Ni. It is suggested[50] that ^{60}Ni might be better suited than other even-A nickel isotopes to a theoretical description based on the spherical shell model. Especially the excitation energies predicted by Auerbach for three excited 0^+ states in ^{60}Ni agree quite well with the observed ones, identified after the calculations.

In the following the electromagnetic decay properties of excited 0^+ states in nickel isotopes are discussed in terms of the available shell-model predictions. The 0^+ states featuring similar decay characteristics are discussed together.

^{58}Ni(0^+_2) and ^{60}Ni(0^+_4) states

The 0^+_2 state in ^{58}Ni and the 0^+_4 state in ^{60}Ni are characterized by strongly hindered $E2(0^+ \to 2^+_1)$ transitions, enhanced $E2(0^+ \to 2^+_2)$ transitions and rather strong $M1(0^+ \to 1^+_1)$ transitions. Consequently, the 0^+_2 state in ^{58}Ni cannot be interpreted as a two-phonon state. More likely these 0^+ states could be discussed as three-phonon states. However, the assumed three-phonon states are strongly pushed down in energy, the ratio $E(0^+_i)/E(2^+_1)$ being 2.02 and 2.69 for ^{58}Ni and ^{60}Ni, respectively. The $E(0^+)/E(2^+_1)$ energy ratios and the $E2(0^+ \to 2^+_{1,2})$ and

$E0(0^+ \rightarrow 0_1^+)$ decay characteristics of these states are quite similar to those observed in our recent work[4,7] for the assumed three-phonon 0_3^+ states in ^{112}Cd and ^{114}Cd. However, clear differences are the strong $M1(0^+ \rightarrow 1_1^+)$ transitions observed in ^{58}Ni and ^{60}Ni and the $E0(0_3^+ \rightarrow 0_2^+)$ transitions observed in ^{112}Cd and ^{114}Cd. It should be noted that there is no sign of a two-phonon state in ^{58}Ni.

A simple shell-model can explain the fact that the monopole strength for the $0_2^+ \rightarrow 0_1^+$ transition in ^{58}Ni is small. The f-p shell-model calculations also quite reasonably predict the energy-level schemes for the nickel isotopes. The shell-model prediction[73] of $B(E2; 0_2^+ \rightarrow 2_2^+)$ = 18 W.u. for ^{58}Ni agrees reasonably with the experimental value of 12(2) W.u. The theoretical value is obtained using a neutron effective charge of $e_n \approx 1.9$ e. This e_n value is larger than the physically realistic upper limit of 1.14 theoretically estimated by Federman et al.[74].

However, all these calculations fail to reproduce the observed retardation of the $E2(0_2^+ \rightarrow 2_1^+)$ transition in ^{58}Ni. The theoretical values are about 10^4 times higher than the experimental value of $B(E2) = 2.6(5) \times 10^{-4}$ W.u. The existing theoretical calculations cannot either explain the rather strong decay branch of the 0_2^+ state via an M1 transition to the 1_1^+ state. The structure of this state is still a puzzle; it has been suggested, e.g., that it might be deformed[73]. For the 0_4^+ state in ^{60}Ni, identified in the present work, there are no shell-model predictions concerning the E2 and M1 transition rates.

$^{60}Ni(0_2^+)$ and $^{62}Ni(0_2^+)$ states

The 0_2^+ states in ^{60}Ni and ^{62}Ni appear to have some two-phonon-like characteristics, such as enhanced $E2(0_2^+ \rightarrow 2_1^+)$ transitions and relatively strong $E0(0_2^+ \rightarrow 0_1^+)$ transitions. The ratios of the reduced transition probabilities X(E0/E2) for these states are quite close to the theoretical values for a spherical vibrator[69] for which $X_{vibr} = \beta_{rms}^2 \approx 0.039$, where β_{rms} is taken from ref. 70. The monopole strength $\rho^2(E0)$ for the $^{62}Ni(0_2^+ \rightarrow 0_1^+)$ transition exceeds the value for a spherical vibrator[69], for which $\rho_{vibr}^2 = (0.151\ Z\beta_{rms}^2)^2 \approx 27 \times 10^{-3}$, by a factor of four. Experimental limits given in table 4 for the half-life of the $^{60}Ni(0_2^+)$ state correspond to a monopole strength of $0.04\ \rho_{vibr}^2 < \rho^2 \leq \rho_{vibr}^2$.

Ballini et al.[61] have suggested that the 0_2^+ state in ^{60}Ni might be the 0^+ basis of a deformed rotational band, similar to those observed in ^{16}O and ^{40}Ca. The present results and the previous measurements of Rauch et al.[76], which establish that at least five levels decay to the 0_2^+ state, do not support such an assumption.

Shell-model calculations by Kennedy et al.[77] have shown that the first 0^+ state in ^{62}Ni occurs at about 2.1 MeV in good agreement with the observed excitation energy. However, the experimental B(E2) value of 100(55) W.u. for the $E2(0_2^+ \rightarrow 2_1^+)$ gamma decay is poorly reproduced in their calculations, which yield B(E2) = 2.4 W.u. with an effective neutron charge of 1.7 e. This enhanced E2 transition rate and the enhanced E0 strength (0.49 s.p.u.) for the $0_2^+ \rightarrow 0_1^+$ internal-pair decay indicate larger contribution of core-excited configurations in the structure of the 0_2^+ state in ^{62}Ni as compared to the $^{60}Ni(0_2^+)$ state.

$^{58}Ni(0_3^+)$ and $^{60}Ni(0_3^+)$ states

The 0_3^+ states in ^{58}Ni and ^{60}Ni have almost equal decay properties: enhanced $E2(0_3^+ \to 2_1^+)$ transitions ($B(E2) \approx 5.5$ W.u.) and intense $E0(0_3^+ \to 0_1^+)$ transitions ($\rho^2(E0) \approx 80 \times 10^{-3}$). The shell-model calculations of Start et al.[78] employing an effective charge of 1.0 e on each valence neutron gave a value of $B(E2) \approx 0.33$ W.u. for the $E2(0_3^+ - 2_1^+)$ transition in ^{58}Ni. It is evident that the observed enhancement cannot be reproduced without assuming core excitation.

The 0_3^+ states in ^{58}Ni and ^{60}Ni are strongly excited in the (^{3}He,n) and (^{6}Li,d) reactions[65,66], but are either extremely weak or not observed at all in (t,p) and (p,t) studies[67,79,80]. A similar strong L = 0 transition to the 0_2^+ state in several Cd and Sn isotopes was observed in a recent (^{3}He,n) study[81]. The (^{3}He,n) results and the observed decay properties[4,6,7] indicate that proton excitations play an important role in these states. According to the pairing-vibrational model[82] the 0_3^+ states in ^{58}Ni and ^{60}Ni could be interpreted as 2p-2h proton-pairing-vibrational states for the Z = 28 closed shell.

The exceptionally intense $E0(0_3^+ \to 0_2^+)$ transitions observed in Sn and Cd isotopes[4,6,7] are interpreted in the framework of deformation and configuration mixing: large $\rho^2(E0)$ values are explained by a strong mixing of components with different shapes in the wave functions of the 0_2^+ and 0_3^+ states.

No E0 transitions between excited 0^+ states are observed in Ni isotopes. An upper limit of $I(E0; 0_3^+ - 0_2^+)/I(E0; 0_3^+ \to 0_1^+) < 0.04$ was deduced from the present internal-pair and conversion-electron measurements for the 0_3^+ state in ^{58}Ni. However, the corresponding upper limit of $\rho^2(0_3^+ \to 0_2^+) < 1.8$ does not allow any conclusions on the structure of these states.

5. SUMMARY

The results presented in this thesis clearly demonstrate that a combination magnetic plus Si(Li)-Si(Li) sum-coincidence technique provides a powerful spectroscopic instrument for obtaining nuclear-structure information from the studies of internal-pair transitions. The main advantages gained over the previous methods are (i) an excellent energy resolution of the sum-coincidence pair lines (4-6 keV) obtained with the aid of cooled, high-resolution Si(Li) detectors and (ii) a high pair-line efficiency ($\approx 10^{-3}$) provided by high transmission and a broad momentum band width of the magnetic lens. Both of the advantages (i) and (ii) are achieved for the first time in the same device. The most serious limiting factor is the background due to random coincidence; the maximum acceptable single-detector counting rate is typically below 3×10^3 cps.

The new technique rendered it possible to obtain results, such as those presented in sect. 4.3., most of which could not have been observed employing the previous methods. The first extensive systematic investigation of the E0 decay branches was carried out in ^{58,60,62}Ni. The present internal-pair measurements confirmed the 0_3^+ assignment of the 3530.9 keV state in ^{58}Ni and the 3318.3 keV state in ^{60}Ni, and yielded a spin and parity assignment of 0_4^+ for the 3588.0 keV state in ^{60}Ni. The E0 ground-state decay branches were determined for these 0^+ states and for the 0_2^+ states in ^{58}Ni, ^{60}Ni and ^{62}Ni.

Shell-model calculations based on the inert ^{56}Ni core valence neutrons occupying the $2p_{3/2}$, $2p_{1/2}$ and $1f_{5/2}$ orbits predict rather reasonably the excitation energies of the 0^+ states. However, all

these calculations fail to reproduce the observed M1($0^+_i \rightarrow 1^+_1$) and E2($0^+_i \rightarrow 2^+_1$) transition rates, even if large e_n values (1.7-1.9 e) are used. The experimental results indicate that the excitation of protons from the $f_{7/2}$ shell has to be included before any significant reduction of the neutron effective charge would result.

So far, there are no calculations to explain the E0 transition rates observed in this work. Especially, the structure of the 0^+_2 state in ^{58}Ni and of the 0^+_4 state in ^{60}Ni is still a puzzle and an explanation of their strong M1 decays to the 1^+_1 states is missing. The decay of the 0^+_2 states in ^{60}Ni and ^{62}Ni is qualitatively in accordance with the naive spherical vibrator if these states are interpreted as two-phonon states. Strong E0($0^+_3 \rightarrow 0^+_1$) transitions in ^{58}Ni and ^{60}Ni indicate that proton excitations play an important role in the structure of the 0^+_3 states. This assumption is supported by the recent (^{3}He,n) and (^{6}Li,d) studies[65,66].

More experimental data on the properties of 0^+ states would give a better basis for systematic theoretical studies of the structure of 0^+ states in the f-p shell. Particularly interesting would be be the measurements on E0 decay branches in the doubly magic $^{56}_{28}Ni_{28}$ and in the neighbouring nuclei $^{54\text{-}58}$Fe and $^{60\text{-}66}$Zn. Work on these nuclei is in progress by the Jyväskylä monopole group.

Appendix I

Comparison between $\Omega_K(E0)$ values calculated by Hager and Seltzer[22] and Bell et al.[23] and those computed[20] in this wprk for atomic numbers Z = 30, 40 and transition energies $k \geq 1$.

Z = 40

$k[m_0c^2]$	Ref. 1	Ref. 2	Ref. 3
1.0	0.538×10^{9}	0.540×10^{9}	0.539×10^{9}
2.0	0.106×10^{10}	0.108×10^{10}	0.108×10^{10}
3.0	0.176×10^{10}	0.178×10^{10}	0.177×10^{10}
4.0	0.258×10^{10}	0.266×10^{10}	0.263×10^{10}
5.0	-	0.369×10^{10}	0.364×10^{10}
6.0	-	-	0.480×10^{10}
7.0	-	-	0.611×10^{10}
8.0	-	-	0.758×10^{10}

Z = 30

$k[m_0c^2]$	Ref. 1	Ref. 2	Ref. 3
1.0	0.803×10^{8}	-	0.801×10^{8}
2.0	0.165×10^{9}	-	0.163×10^{9}
3.0	0.276×10^{9}	-	0.273×10^{9}
4.0	0.407×10^{9}	-	0.407×10^{9}
5.0	-	-	0.568×10^{9}
6.0	-	-	0.754×10^{9}
7.0	-	-	0.965×10^{9}
8.0	-	-	0.120×10^{10}

Appendix II

The differential internal-pair-formation coefficients $\gamma_\ell(\Theta,W_+)$ are for electric moncpole transitions[29]

$$\gamma_{E0}(\Theta,W_+) = \frac{p_+p_-(W_+W_- - 1 + p_+p_- \cos\Theta)}{4\ I(E0)}$$

and for electric and magnetic multipoles[24]

$$\gamma_{E\ell}(\Theta,W_+) = \frac{2\alpha}{\pi(\ell+1)} \times \frac{p_+p_-}{q} \times \frac{(q/k)^{2\ell-1}}{(k^2-q^2)^2} \times \Big\{ (2\ell+1)(W_+W_- + 1 - \frac{1}{3} p_+p_- \cos\Theta) + \ell\,[(q^2/k^2) - 2](W_+W_- - 1 + p_+p_- \cos\Theta)$$

$$+ \frac{1}{3}(\ell-1)p_+p_-\,[(3/q^2)\,(p_- + p_+ \cos\Theta) \times (p_+ + p_- \cos\Theta) - \cos\Theta]\Big\},$$

$$\gamma_{M\ell}(\Theta,W_+) = \frac{2\alpha}{\pi} \times \frac{p_+p_-}{q} \times \frac{(q/k)^{2\ell+1}}{(k^2-q^2)^2} \times \Big\{ 1 + W_+W_- - \frac{p_+p_-}{q^2}\,(p_- + p_+ \cos\Theta)(p_+ + p_- \cos\Theta)\Big\},$$

where

$W_+ + W_- = k$ (in units of m_0c^2), $p_\pm = (W_\pm^2 - 1)^{1/2}$, $q^2 = p_+^2 + p_-^2 + 2p_+p_- \cos\Theta$, $I(E0) = \int_1^{k/2} \Big\{ [(k-W)^2-1](W^2-1) \Big\}^{1/2}$

$$\times\ [(k-W)^2-1]\,dW.$$

Appendix III

The expressions for $\gamma_\ell(\Theta,k)$ for the required condition $W_+ = W_- = \frac{1}{2}k$ are the following:

$$\gamma_{E0}(\Theta,k) = \frac{(\frac{1}{4}k^2 - 1)^2(1 + \cos\Theta)}{4\ I(E0)},$$

$$\gamma_{E\ell}(\Theta,k) = \frac{2^{2\ell-5}(\frac{1}{4}k^2 - 1)^{\ell-2}}{\pi(137)(\ell+1)k^{2\ell-1}[1/(\frac{1}{4}k^2-1)+1-\cos^2\frac{1}{2}\Theta)]^2} \times \left\{ [(3\ell+1)(\tfrac{1}{4}k^2)+\ell+1]\ [\cos^2\tfrac{1}{2}\Theta]^{\ell-1} - (5\ell+1)(\tfrac{1}{4}k^2-1)[\cos^2\tfrac{1}{2}\Theta]^{\ell} + (8\ell/k^2)(\tfrac{1}{4}k^2-1)^2\ [\cos^2\tfrac{1}{2}\Theta]^{\ell+1} \right\},$$

$$\gamma_{M\ell}(\Theta,k) = \frac{2^{2\ell-3}(\frac{1}{4}k^2 - 1)^{\ell-1}}{\pi(137)k^{2\ell+1}[1/(\frac{1}{4}k^2-1)+1-\cos^2\frac{1}{2}\Theta]^2} \times \left\{ (\tfrac{1}{4}k^2+1)\ [\cos^2\tfrac{1}{2}\Theta]^{\ell} - (\tfrac{1}{4}k^2-1)\ [\cos^2\tfrac{1}{2}\Theta]^{\ell+1} \right\}.$$

References

1) J. Kantele, M. Luontama, A. Passoja and R. Julin, Nucl. Instr. and Meth. 130 (1975) 467

2) M. Luontama, J. Kantele, R. Julin, A. Passoja, T. Poikolainen and M. Pylvänäinen, Nucl. Instr. and Meth. 159 (1979) 339

3) R. Julin, J. Kantele, M. Luontama, A. Passoja and T. Poikolainen, Nucl. Instr. and Meth. 152 (1978) 471

4) R. Julin, Ph.D. thesis, University of Jyväskylä, Finland, unpublished

5) R. Julin, J. Kantele, M. Luontama, T. Poikolainen and V. Rahkonen, Phys. Lett. 65B (1976) 337

6) A. Bäcklin, W. Dietrich, R. Julin, J. Kantele, M. Luontama and L. Westerberg, Phys. Lett. 62B (1976) 402;
J. Kantele, R. Julin, M. Luontama, A. Passoja, T. Poikolainen, A. Bäcklin and N.-G. Jonsson, Z. Physik A289 (1979) 157

7) A. Bäcklin, N.-G. Jonsson, R. Julin, J. Kantele, M. Luontama, A. Passoja and T. Poikolainen, UUIP-999, Institute of Physics, University of Uppsala, and to be published;
R. Julin, J. Kantele, M. Luontama, A. Passoja, T. Poikolainen, A. Bäcklin and N.-G. Jonsson, JYFL Annual Report 1978, 3.8., and to be published

8) R. Julin, J. Kantele, M. Luontama, A. Passoja, P. Kleinheinz and J. Blomqvist, JYFL Annual Report 1979, 3.14., and to be published

9) S. Cohen, R.D. Lawson, M.H. Macfarlane, S.P. Pandya and M. Soga, Phys. Rev. 160 (1967) 903

10) N. Auerbach, Phys. Rev. 163 (1967) 1203

11) P.W.M. Glaudemans, M.J.A. deVoigt and E.F.M. Steffens, Nucl. Phys. A198 (1972) 609

12) J.E. Koops and P.W.M. Glaudemans, Z. Physik A280 (1977) 181 and references therein

13) N.A. Voinova, The 0^+ states and electric monopole transitions in even-even atomic nuclei, INDC (CCP)-93/N, IAEA, Vienna, 1976

14) E.K. Warburton and D.E. Alburger, Phys. Lett. 36B (1971) 38

15) A. Passoja, J. Kantele, M. Luontama and R. Julin, Nucl. Instr. and Meth. 157 (1978) 513

16) A. Passoja, J. Kantele, R. Julin and M. Luontama, Nucl. Instr. and Meth. 166 (1979) 203

17) E.L. Church and J. Weneser, Phys. Rev. 103 (1956) 1035

18) R.H. Dalitz, Proc. Roy. Soc. A206 (1951) 521

19) D.H. Wilkinson, Nucl. Phys. A133 (1969) 1

20) A. Passoja, JYFL Research Report, in preparation

21) R.J. Lombard, C.F. Perdrisat and J.H. Brunner, Nucl. Phys. A110 (1968) 41

22) R.S. Hager nad E.C. Seltzer, Nucl. Data Tables A6 (1969) 1

23) D.A. Bell, C.E. Aveledo, M.G. Davidson and J.P. Davidson, Can. J. Phys. 48 (1970) 2542

24) M.E. Rose, Phys. Rev. 76 (1949) 678

25) M.E. Rose, Phys. Rev. 78 (1950) 184

26) M.E. Rose, Phys. Rev. 131 (1963) 1260

27) E.K. Warburton, Phys. Rev. 133 (1964) B1368

28) J.R. Oppenheimer, Phys. Rev. 60 (1941) 164

29) E.K. Warburton, D.E. Alburger, A. Gallmann, P. Wagner and L.F. Chase, Jr., Phys. Rev. 133 (1964) B42

30) W. Michaelis, D. Lange and Gl Wilhelmi, Proc. Int. Symp. on Neutron Capture Gamma-Ray Spectroscopy, Studsvik, 11-15 Aug. 1969 (IAEA, Vienna, 1969)

31) R. Pepelnik, U. Fanger and W. Michaelis, Nucl. Instr. and Meth. 115 (1974) 285 and references therein

32) Table of isotopes, ed. by C.M. Lederer and V.S. Shirley, 7th ed. (Wiley, New York, 1978)

33) D.C. Kocher and R.L. Auble, Nucl. Data Sheets 19 (1976) 445

34) R.L. Auble, Nucl. Data Sheets 28 (1979) 103

35) M.L. Halbert, Nucl. Data Sheets 26 (1979) 5

36) P. Kleinheinz, L. Samuelson, R. Vukanovič and K. Siegbahn, Nucl. Instr. and Meth. 32 (1965) 1

37) M.J. Berger, S.M. Seltzer, S.E. Chappell, J.C. Humphreys and J.W. Motz, Nucl. Instr. and Meth. 69 (1969) 181

38) A review is given by R. Wilson, in Alpha-, beta- and gamma-ray spectroscopy, ed. K. Siegbahn (North-Holland, Amsterdam, 1965)

39) H. Daniel and W. Bothe, Zeits. für Naturforsch. 9a (1954) 402

40) R. Bent, T. Bonner and R. Sippel, Phys. Rev. 98 (1955) 1237

41) D. Alburger, Phys. Rev. 111 (1958) 1586

42) J. Kjellman and B. Johansson, Ark. Fys. 14 (1958) 17

43) J.C. Adloff, K.H. Souw, D. Disdier, F. Scheibling, P. Chevallier and Y. Wolfson, Phys. Rev. C 10 (1974) 1819

44) M. Ulrickson, N. Benczer-Koller, J.R. MacDonald and J.W. Tape, Phys. Rev. C 15 (1977) 186 and references therein

45) W. Michaelis and D. Lange, Nucl. Instr. and Meth. 58 (1968) 349

46) W.J. Courtney and C.F. Moore, Phys. Lett. 31B (1970) 131

47) M. Nessin, T.H. Kruse and K.E. Eklund, Phys. Rev. 125 (1962) 639

48) J. Kantele and A. Passoja, Nucl. Instr. and Meth. 92 (1971) 247

49) A. Passoja, R. Julin, J. Kantele and M. Luontama, JYFL Annual Report 1978, 1.2.4., unpublished

50) C. Moazed, T. Becker, P.A. Assimakopoulos and D.M. van Patter, Nucl. Phys. A169 (1971) 651

51) N.B. Gove and A.H. Wapstra, Nucl. Data Tables 11 (1972) 127

52) B.N. Belyaev, Soviet J. Nucl. Phys., 14 (1972) 641

53) B.N. Belyaev, Bull. Acad. Sci. USSR, Phys. Ser. 36 (1972) 1928

54) D.H. Wilkinson, D.E. Alburger, E.K. Warburton and R. Pixley, Phys. Rev. 129 (1963) 1643

55) E.K. Warburton, D.E. Alburger and D.H. Wilkinson, Phys. Rev. 132 (1963) 776

56) R.D. Bent, T.W. Bonner, J.H. MacCrary, W.A. Ranken and R.F. Sippel, Phys. Rev. 99 (1955) 710

57) G.A. Bartholomew and G.E. Lee-Whiting, Nucl. Instr. and Meth. 162 (1979) 239

58) E.K. Warburton and D.E. Alburger, Phys. Rev. C 6 (1972) 1224

59) I.M. Band, M.B. Trzhaskovskaya and M.A. Listengarten, Atomic Data and Nucl. Data Tables 18 (1976) 433

60) L.S. Hsu and J.B. French, Phys. Lett. 19 (1965) 135

61) R. Ballini, A.G. Blair, N. Cindro, J. Delaunay and J.P. Fouan, Nucl. Phys. A111 (1968) 147

62) M.R. Gunye and S.B. Khadkikar, Phys. Lett. 30 (1969) 609

63) H.D. Gräf, H. Feldmeier, P. Manakos, A. Richter and E. Spamer, Nucl. Phys. A295 (1978) 319 and references therein

64) P.V.M. Glaudemans, private communication (1979)

65) N.Stein, J.W. Sunier and C.W. Woods, Phys. Rev. Lett. 38 (1977) 587

66) W.P. Alford, R.A. Lindgren, D. Elmore and R.N. Boyd, Nucl. Phys. A243 (1975) 269

67) W. Darcey, R. Chapman and S. Hinds, Nucl. Phys. A170 (1971) 253

68) D.H. Kong-A-Siou and H. Nann, Phys. Rev. C 11 (1975) 1681

69) H. Kumar, in The electromagnetic interaction in nuclear spectroscopy, ed. W.D. Hamilton (North-Holland, Amsterdam, 1975) ch. 3

70) P.H. Stelson and L. Grodzins, Nucl. Data A1 (1965) 21

71) K.H. Souw, J.C. Adloff, D. Disdier and P. Chevallier, Phys. Rev. C 12 (1975) 1103

72) T. Suehiro, Y. Ishizaki, H. Ogata, J. Kokame, Y. Saji, A. Stricker, Y. Sugiyama and I. Nonaka, Phys. Lett. 33B (1970) 468

73) S. Raman, Nucl. Phys. A158 (1970) 65

74) P. Federman and L. Zamick, Phys. Rev. 177 (1969) 1534

75) W.S. Gray, P.J. Ellis, T. Wei, R.M. Polichar and J. Jänecke, Nucl. Phys. A140 (1970) 494

76) F. Rauch, D.M. van Patter and P.F. Hinrichsen, Nucl. Phys. A124 (1969) 145

77) D.L. Kennedy, H.H. Bolotin, I. Morrison and K. Amos, Nucl. Phys. A308 (1978) 14

78) D.F. Start, R. Anderson, L.E. Carlson, A.G. Robertson and M.A. Grace, Nucl. Phys. A162 (1971) 49

79) G. Bassini, N. Hintz and C.D. Kavaloski, Phys. Rev. 136 (1964) B1006

80) W.G. Davies, J.E. Kitching, W. MacLatchie, J. Morton, D.G. Montague, K. Ramavataram, N.S. Chant, T.A. Hodges, F. Uridge and D.A. Morris, Rutherford High Energy Laboratory Progress Report (Nov. 12, 1968) unpublished

81) H.W. Fielding, R.E. Anderson, C.D. Zafiratos, D.A. Lind, F.E. Cecil, H.H. Wieman and W.P. Alford, Nucl. Phys. A281 (1977) 389

82) First proposed by A. Bohr (p. 179) and O. Nathan (p. 191), in Nuclear Structure (International Atomic Energy Agency, Vienna, 1968)